LC-MS based characterization of *Mycobacterium tuberculosis* shikimate kinase inhibitors containing oxadiazole-amide and aminobenzothiazole rings

by

Mansour S. Alturki

A thesis submitted to the Graduate Faculty of
Auburn University
in partial fulfillment of the
requirements for the Degree of
Master of Science

Auburn, Alabama
August 06, 2016

Keywords: liquid-chromatography, mass spectrometry, tuberculosis,
Mycobacterium tuberculosis, shikimate kinase, shikimate-3-phosphate.

Approved by

Angela I. Calderón, Chair, Associate Professor of Drug Discovery and Development
Randall Clark, Professor of Drug Discovery and Development
Jack DeRuiter, Professor of Drug Discovery and Development
Forrest Smith, Associate Professor of Drug Discovery and Development

Abstract

The emergence of multidrug-resistant tuberculosis (MDR-TB) and extensively drug-resistant tuberculosis (XDR-TB) has increased the demand for the discovery of new antitubercular drugs. The shikimate pathway is essential for the survival of *Mycobacterium tuberculosis* (*Mtb*), due to the production of chorismate, a precursor for aromatic amino acids but is absent from mammals. Shikimate kinase (SK) the fifth enzyme in the shikimate pathway in *Mtb* that catalyzes a phosphate transfer from ATP to shikimate, producing shikimate-3-phosphate (S3P) and ADP, and has been considered a promising drug target for tuberculosis drug discovery. The goal of this thesis is to understand the inhibitory mechanism of the most active compounds from a set of 14 oxadiazole-amide and 2-aminobenzothiazole containing synthetic compounds with IC_{50} values <50 µM against *Mycobacterium tuberculosis* shikimate kinase (*Mt*SK) using an LC-MS based approach.

Chapter one is an overview of tuberculosis pathogenesis and statistics, and it describes the role of the shikimate pathway in *M. tuberculosis* (*Mtb*). Additionally, this chapter describes a short revision of specific and non-specific binding to drug targets, *Mtb* cell wall permeability, and antibacterial activity of 1,3,4-oxadiazole, and 2-aminobenzothiazole scaffolds.

Chapter two describes the experimental characterization of *M. tuberculosis* shikimate kinase inhibitors containing oxadiazole-amide and aminobenzothiazole rings by using LC-MS and other orthogonal confirmatory assays.

Chapter three describes the results, discussion and conclusions. Our findings by the use of LC-MS, ^{1}H-NMR, DLS, TEM, and centrifugation assays suggested that these compounds are non-specific inhibitors of *Mt*SK by aggregate formation.

Table of Contents

List of Figures

List of Tables

List of Abbreviations

μL	Microliter
μM	Micromolar
°C	Degree centigrade
ADP	Adenosine diphosphate
ATP	Adenosine triphosphate
cLogP	Calculated logarithm of compound's partition coefficient between n-octanol and water
CM	Chorismate mutase
CS	Chorismate synthase
DC	Dendritic cell
DLS	Dynamic light scattering
DMSO	Dimethyl sulfoxide
EIC	Extracted ion chromatogram
ESI	Electrospray ionization
FOSA	hydrophobic part of the solvent accessible surface area (saturated carbon and attached hydrogen atoms)
accptHB	Number of hydrogen bond acceptors
kDa	Kilodalton
LC-MS	Liquid chromatography-mass spectrometry
MDR	Multi drug-resistant
mL	Milliliter

MS   Mass spectrometry

Mtb   *Mycobacterium tuberculosis*

*Mt*SK   *Mycobacterium tuberculosis* shikimate kinase

nm   Nanometer

NMR   Nuclear magnetic resonance

Q-TOF   Quadrupole Time-of-flight

PAINS   Pan-assay interference compounds

Phe   Phenylalanin

PISA   Portion of the solvent accessible surface area responsible for π interaction

PTA   Phosphotungstic acid

S3P   Shikimate-3-phosphate

SK   Shikimate kinase

TB   Tuberculosis

TEM   Transmission electronic microscopy

Trp   Tryptophan

Tyr   Tyrosine

v/v   Volume/volume

XDR   Extensively drug-resistant

Chapter 1: Literature review

1.1 Introduction

Globally, *Tuberculosis* (TB) is a leading cause of mortality next by a bacterial infection second only to HIV. There were 1.5 million TB deaths and approximately 9.6 million new TB cases in 2014 [1]. *Tuberculosis* is a contagious infectious disease caused by the intracellular pathogen *Mycobacterium tuberculosis* (*Mtb*). It can produce an active disease or a latent infection with or without clinical manifestations, respectively. It mainly affects the lungs (pulmonary TB) but can affect other sites as well (extrapulmonary TB). *Mtb* can be transmitted between individuals by coughing or sneezing (Fig. 1.1) [2]. Inside the infected host, the bacteria are phagocytized by alveolar macrophages, which result in triggering immune response cells, including chemokines and cytokines [3]. The formation of granulomas that surrounds *Mtb* is the outcome of the activation of adaptive immune response, dendritic cells (DCs), activated macrophages and other leukocytes, including neutrophils, and monocytes; consequently, the majority of the mycobacteria are eradicated, but not completely destroyed [4]. *Mtb* can disseminate to different regions in the body and cause extrapulmonary TB disease, including the brain, larynx, lymph nodes, pleura, kidneys, bones, and joints [5]. After the containment of *Mtb* by immune response cells, *Mtb* shifts to a silent (inactive) mode, which is called latent TB. At this stage, the bacteria can reside inside the granulomas and endure host defense [6]. Once the immune system becomes compromised due to either HIV, diabetes mellitus, malnutrition, smoking, or immune suppression, the opportunistic bacteria become reactivated and cause illness to the host [7,8].

Droplet nuclei containing tubercle bacilli are inhaled, enter the lungs, and travel to the alveoli.

Bronchiol
Tubercle
Alveoli

Brain
Bone
Larynx
Lymph node
Lung
Spine
Kidney

Tubercle bacilli multiply in the alveoli.

A small number of tubercle bacilli enter the bloodstream and spread throughout the body.

Special immune cells form a barrier shell

Shell breaks down and tubercle bacilli escape and multiply

Macrophages ingest and surround the tubercle bacilli, which form a granuloma, that keeps the bacilli contained and under control Latent Tuberculosis Infection (LTBI).

If the immune system cannot keep the tubercle bacilli under control, the bacilli begin to multiply rapidly (TB disease).

Figure 1.1. Tuberculosis pathogenesis [2].

1.2 Shikimate kinase from *Mycobacterium tuberculosis*

Genomic studies have revealed metabolic pathways in the mycobacteria, which are considered as drug targets, encompassing lipid metabolism, carbohydrate metabolism, amino acid metabolism, energy metabolism, vitamin and cofactor biosynthetic pathways and nucleotide metabolism [9,10]. Furthermore, specific enzymes, which are present in a certain metabolic pathway in *Mycobacterium tuberculosis* (*Mtb*) but absent in the host, could represent a promising drug target such as shikimate kinase (SK) [11].

The shikimate pathway is essential for *Mtb* survival, due to the production of chorismate, a precursor for aromatic amino acids phenylalanine, tyrosine, and tryptophan but absent from mammals (Fig. 1.2). Evidently, the disruption of this pathway will lead to protein synthesis inhibition and the death of *Mtb* [12]. Shikimate kinase (SK) (EC 2.7.1.71) is the fifth enzyme in the shikimate pathway an it catalyzes a phosphate transfer from ATP to shikimate, producing shikimate-3-phosphate (S3P) and ADP (Fig. 1.3), and has been considered a promising drug target for tuberculosis drug discovery [12].

Mycobacterium tuberculosis shikimate kinase (*Mt*SK) is an 18.5 kDa protein, which is encoded by the *aroK* gene and made of 531 bp and176 amino acids [13]. Gene disruption studies have displayed that *Mt*SK is crucial for the viability of *Mtb* [14]. Consequently, it could serve as a promising target for the discovery of antitubercular agents targeting either ATP or shikimate-binding sites.
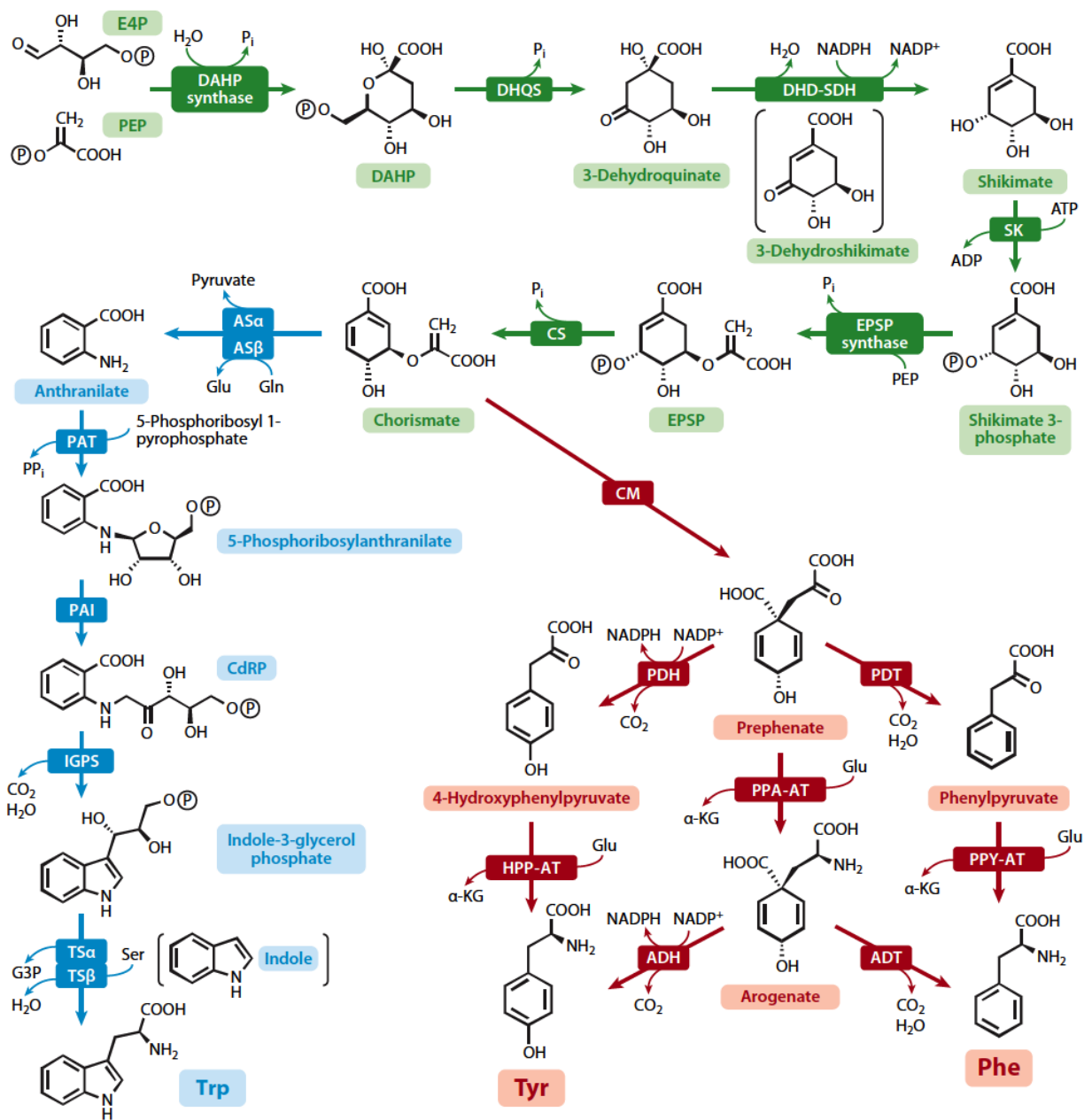
Figure 1.2. The shikimate pathway. [15]
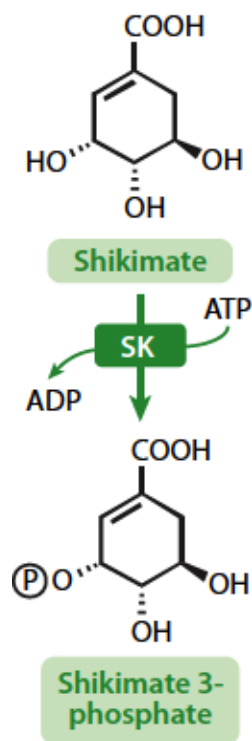
Figure 1.3. Shikimate kinase catalyzed reaction. [15]

Similar to any kinase enzyme, SK belongs to the family of nucleoside monophosphate (NMP) kinases [13] and consists of a central five-stranded parallel β -sheet surrounded by eight helices [16].

The structure of SK has three domains: the lid domain (LID) (residues 112-124) which contains catalytic and substrate binding residues and closes over the substrate binding pockets upon substrate binding, shikimate-binding domain (SBD) (residues 32-61) that corresponds to the NMP-binding domain in NMP kinases, and ATP-binding domain (ABD), Upon binding of either substrate, a closed conformation characterized by closure of the LID domain over the active site is observed (Fig. 1.4) [16]. The nucleotide binding (NB) site and the LID domain are flexible regions of the structures that are responsible for movement [17]. Shikimate binding results in a rotation of the SB domain into the substrate binding pocket and ATP binding induces a rotation of the NB

domain into the substrate binding pocket, and the binding of one substrate is thought to synergistically enhance the affinity for the second substrate (positive cooperativity) [16, 18].
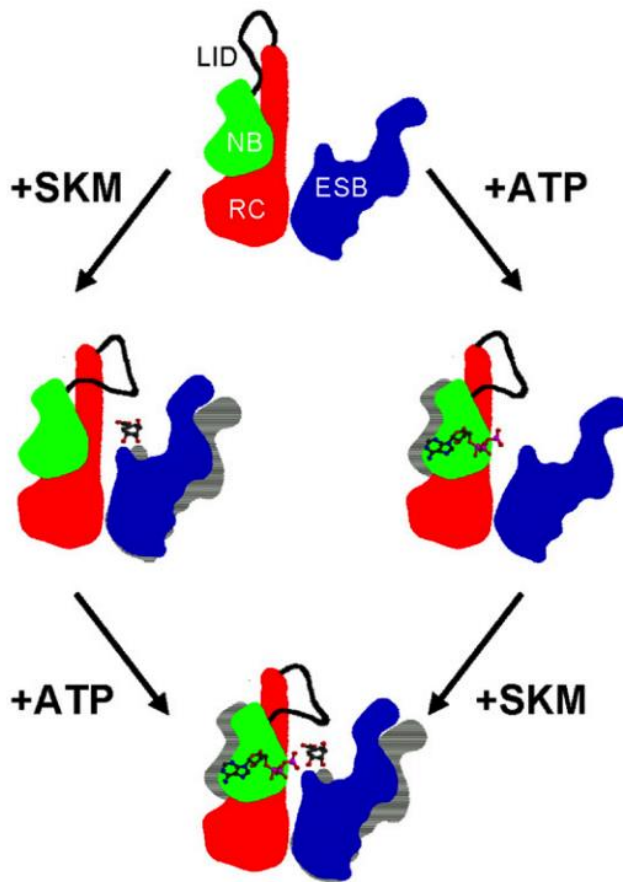
Figure 1.4. Conformational changes of shikimate kinase upon substrate binding. The LID domain is shown in black, the extended shikimate-binding domain (ESB) is shown in blue, the nucleotide-binding domain is shown in green and the reduced core (RC) is shown in red. Upon binding of either shikimate or ATP to the ESB or NB domains, respectively, movement of the LID domain over the active site is witnessed [16].

1.3 Specific and non-specific binding to drug targets

Discovering a potential inhibitor requires the successful identification of a lead compound from the drug discovery pipeline. Identification of a legitimate hit is an essential stage toward the generation of a lead compound. This can be achieved in different ways, including screening of compound libraries against a biological target [19]. High throughput screening (HTS) is commonly used to identify active compounds; however, this process could yield false positive active compounds. An essential part to generate hits is the identification of specific binding between compounds and their targets, including enzymes, and receptors, through reversible or irreversible interactions (Fig. 1.5) [18]. These interactions are pharmacologically tractable and can lead to target based drug discovery, which is an important strategy for developing new therapeutic agents [20]. Also, such interactions would delineate the mechanism of inhibition of a particular enzyme in many diseases [21].
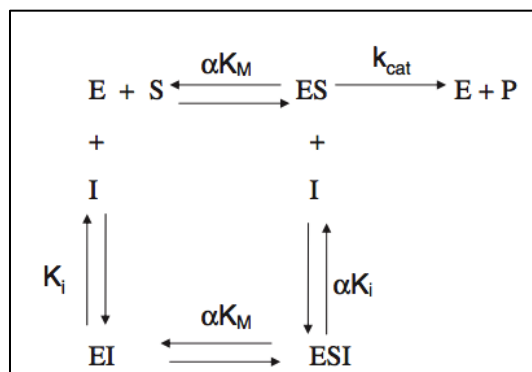
Figure 1.5. Kinetic scheme for reversible enzyme inhibitor [18].

There are compound classes that are commonly found in large compound libraries, and they inhibit proteins non-specifically, involving redox reaction, metal ion chelation, covalent modulation, and aggregate formation [22]. Baell and Holloway have previously described these types of molecules as pan-assay interference compounds (PAINS), which they show false positive results [23]. Unfortunately, these problematic compounds continue to be prevalent in early

discovery campaigns [23]. They usually show false positive read outs in high throughput screening (HTS). Although sometimes they are not easily discovered, luckily, compounds with certain problematic functionalities can be recognized and excluded in an early drug discovery process by using PAINS and other well-known filters [23-25]. However, there is another set of compounds that are troublesome for medicinal chemists; they are not flagged by reactive compounds filters, complied with Lipinski guidelines, shared characteristics of active compounds, and showed similar results in different assays [26]. They are known to display steep concentration-response curves, high Hill Slope [27], ambiguous structure-activity relationships (SAR) [28], and large particles with different sizes in the aqueous solution [29]. They display aggregate or colloidal formation in buffer solutions and inhibit enzymes by three mechanisms, including partial unfolding, restrained dynamics, and physical sequestration (Fig. 1.6) [30]. Unlike true inhibitors, aggregators are affected by enzyme concentration, displayed non-competitive inhibition, non-specific to a single target, often time-dependent but reversible inhibition, and sensitive upon addition of detergents [31-35]. Consequently, these nuisance compounds result in a waste of time, and resources, and they should be excluded from drug discovery programs in a timely manner [22,24,26,28,36].
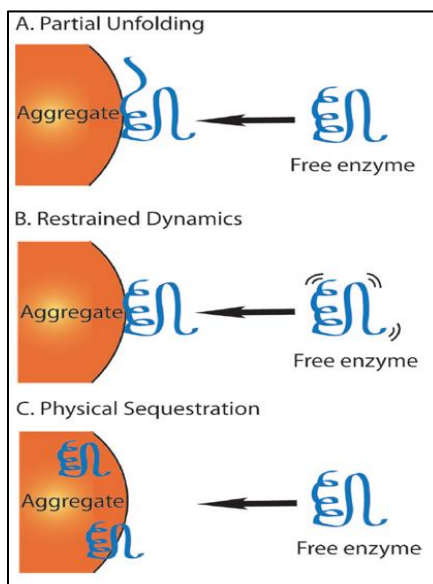
Figure 1.6. Mechanisms of enzyme inhibition by aggregate-based inhibition [30].

1.4 *M. tuberculosis* (*Mtb*) cell wall permeability

Mycobacteria have a rigid cell wall that provides structural integrity and is less permeable to drugs and other nutrients than other microorganisms, which results in antibiotic resistance and slow growth of *Mtb* [37]. Another characteristic of the mycobacterial cell wall that distinguishes it from other bacteria is its ability to retain acid stain, due to the presence of mycolic acid within its cell wall envelope [37]. The cell wall of the mycobacteria is composed of arabinogalactan-peptidoglycan complex and esterified with mycolic acids [38]. Unlike the cell wall composition of other bacteria, the waxy nature of the mycobacteria cell wall due to the presence of mycolic acid and other lipophilic components renders the mycobacteria less permeable to hydrophilic antibiotics. This low permeability results in the delivery of low drug concentration at the site of antitubercular action and increases the risk of drug resistance [39]. Therefore, lipophilic and amphiphilic drugs are believed to traverse the cell wall of the mycobacteria by passive diffusion, simply by dissolving into the highly lipophilic outer layer of the mycobacterial cell wall. On the other hand, the mycobacterial cell displays high intrinsic resistance toward these drugs [40]. In addition, *Mtb* has other means of transportations, including facilitated diffusion like porins, a water-filled open channels. For example, OmpA-like porins are present in *Mtb*, and they allow the permeation of hydrophilic drugs and other hydrophilic nutrients across *Mtb* cell wall [41]. However, the passage rate of the hydrophilic compounds is very slow due to the low number of porins [40]. Generally, lipophilic drugs demonstrated a higher permeability than hydrophilic counterparts in the same class [42].

The genome sequence for *Mtb* has revealed that there is another type of transporters called active transporters, which include influx transporters and efflux pumps. Influx transporters facilitate the entrance of substrates, including sugars, amino acids, metals and anions, whereas,

efflux pumps contribute to exporting drugs outside the cell, which results in *Mtb* drug resistance [43].

Taken all together, there is no single pathway or parameter that contributes to drugs accumulation inside *Mtb*. Instead, it is a blend of different mechanisms, including passive and active transportations and efflux pumps that are all needed to be considered. Therefore, the key success to discovering a novel lead compound against *Mtb* is to understand different drug transporter pathways.

1.5 Antibacterial activity of 1,3,4-oxadiazole scaffold

Generally, compounds containing heterocyclic systems continue to show importance in drug discovery. They gained their significance from being similar to the endogenous molecules in the biological system and natural products, including neurotransmitters, nucleic acids, hormones, vitamins, alkaloids, carbohydrates etc [44]. In addition, they have other beneficial uses, especially in lead optimization by improving binding and activity, increasing or reducing cLogP values, and dissolution [44].

One class of hetero aromatic rings 1,3,4-oxadiazole and its analogues have gained an increase interest because they have shown to display anti-tubercular activity and antibacterial activity against *Staphylococcus aureus*, *Streptococcus faecalis, Bacillus subtilis, Klebsiella pneumoniae, Escherichia coli, and Pseudomonas aeruginosa* [45,47]. Oxadiazoles are a five membered ring compounds, and they possess one oxygen and two nitrogen atoms [46]. In structure activity relationship analysis (SAR), the azole functionality within the ring oxadiazoles improves lipophilicity, allowing the drug to passively diffuse through *Mtb* cell wall [48].

A set of synthetic analogues containing 1,3,4-oxadiazole rings have previously shown to be active against *Mt*SK (Fig. 1.7) [49]. Also, in silico studies reported by Simithy et al. (2014)

have displayed specific interactions of 1,3,4-oxadiazole analogues with *Mt*SK [49]. However, no studies have been done to characterize the mode of inhibition of these analogues.
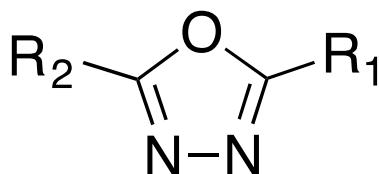
Figure 1.7. 1,3,4-Oxadiazole moiety [49].

1.6 Antibacterial activity of 2-aminobenzothiazole scaffold

In recent years, there has been a sparking interest to discover new antibiotics with potential activity for the treatment of tuberculosis. For this reason, different classes of compounds have been generated, among them, the 2-aminobenzothiazole, which is a unique class of inhibitors and presents among synthetic analogues and natural products [50]. It has a wide range of biological activities, including anti-*Mtb* and against other bacteria, for instance *P. aeruginosa, E. coli, B. subtilis, S. aureus and* methicillin-resistant *Staphylococcus aureus (MRSA)* [51,52]. However, it has been unwell represented in the antibacterial literature [53].

A set of 2-aminobenzothiazole analogous have been described previously to exhibit phenotypic activity against *M. tuberculosis* H37Rv with an IC_{90} less than 3 µg/ml and SI more than 10 [53].

2-Aminobenzothiazole scaffold containing compounds are well-known as kinase inhibitors in different diseases [50, 54]. Therefore, they are considered as a promising candidates against *Mycobacterium tuberculosis* shikimate kinase. Moreover, docking studies have shown specific interactions of 2-aminobenzothiazole analogues with *Mt*SK [49].

Interestingly, a work that has been done by Simithy et al [49]. showed inhibition activity of a set of 2-aminobenzothiazole analogous against MtSK (Fig. 1.8) [49]. However, the mechanism of inhibition of these analogues have not been described, yet.
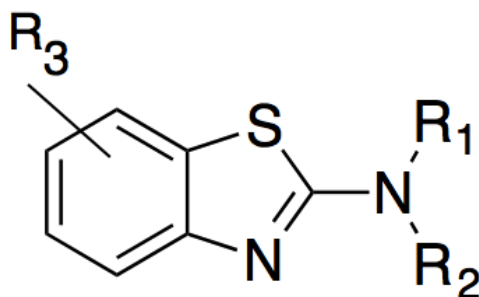
Figure 1.8. 2-Aminobenzothiazole moiety [49].

1.7 Project rationale

Mycobacterium tuberculosis (*Mtb*) is caused by is an infectious bacterial pathogen that replicates primarily in the lungs, causing tuberculosis (TB). *Mtb* It has re-emerged along with HIV as a serious public health threat worldwide because of a significant increase in multiple drug resistance. Worldwide, TB is the leading cause of death of millions of people. The increase in multi-drug resistant (MDR) and extensively-drug resistance (XDR) tuberculosis cases is due to patient non-compliance with long period treatment protocols is a global health concern. Therefore, there is an urgent call for the discovery of new antimycobacterial agents to defeat TB. Analysis of complete genomes has facilitated the identification of potential gene products that are responsible for encoding potential targets, among them is shikimate kinase (SK), which is present in the shikimate pathway in *Mtb* and absent in the host such as humans and animals. The shikimate pathway has been proven to be vital for the survival of *Mtb* because it is responsible for the production of essential aromatic compounds. Accordingly, SK is a promising target for the development of antitubercular agents.

In this work, a target-based approach has been employed by utilizing mass spectrometry to identify the mode of action of a set of 14 synthetic compounds, containing oxadiazole-amide and aminobenzothiazole scaffolds, which have previously shown activity against *Mt*SK. Further, these active compounds have previously displayed phenotypic activity against whole cells of *M. tuberculosis*. Thus, the rationale of this study is to identify the mechanism of inhibition of these hits and their specificity toward the drug target. Therefore, it will lead to the development of antibiotics that are safe, more marketable and cost effective to treat tuberculosis.

1.8 Research objectives

The aim of this project is to characterize the mechanism of inhibition of a set of 14 synthetic inhibitors, containing oxadiazole-amide and aminobenzothiazole scaffolds that have shown to be active against *Mt*SK using LC-MS. The specific goals of this research are to:

1. Screen a set of active synthetic compounds to identify their mechanism of inhibition against *Mt*SK by LC-MS.

2. Determination of specific and non-specific interactions between the **14** synthetic compounds and *Mt*SK by LC-MS.

3. Identify the causes of non-specific interactions between the **14** synthetic compounds and *Mt*SK LC-MS.

4. Confirmation of non-specific *Mt*SK inhibition of the **14** synthetic compounds by orthogonal techniques, encompassing proton nuclear magnetic resonance spectroscopy (^{1}H-NMR), dynamic light scattering (DLS), transmission electronic microscopy (TEM), and centrifugation.

Chapter 2: Experimental characterization of *Mycobacterium tuberculosis* shikimate kinase inhibitors containing oxadiazole-amide and 2-aminobenzothiazole rings

2.1 Introduction

Multi-drug resistant (MDR) strains, extensively drug-resistant (XDR) strains of *Mycobacterium tuberculosis* (*Mtb*), and HIV-TB co-infection are the result of TB epidemic. Although there were many advances in drug discovery and development research, TB remains one of the leading causes of mortality. Therefore, the development of effective and selective drugs with a novel mechanism of action would be in high demand. Also, there is an economic burden on both individuals and communities due to antimicrobial resistance [1, 55].

Since the advent of mass spectrometry (MS), many studies have shown that MS is an important tool to investigate protein-ligand inhibition [56]. MS has a great potential for analyzing non-covalently and covalently associated biomacromolecular complexes [57-59]. Moreover, MS has proven to be more advantageous than other spectrophotometric methods for the characterization of enzyme kinetics and enzyme-ligand inhibition due to its specific, sensitive, and simple analysis [60,61].

The genesis of the set of 14 compounds containing oxadiazole-amide and aminobenzothiazole scaffolds used on this research was from a compound library that consisted of 404 compounds selected from the Tuberculosis Antimicrobial Acquisition and Coordinating Facility (TAACF) Program through National Institute of Allergy and Infectious Diseases (NIAID), which had been screened for growth inhibition in cell culture of *M. tuberculosis* H37Rv by Southern Research Institute (SRI) [53,62,63]. Furthermore, the 404 phenotypically active compounds were further tested in vitro against *M. tuberculosis* shikimate kinase (*Mt*SK) for target

inhibition. Among them, only 14 compounds displayed activity >90 % inhibition and $IC_{50} < 50$ µM, these compounds comprise 1,3,4-oxadiazole-amide and 2-aminobenzothiazole rings [49]. In the current study, the 14 compounds, oxadiazole-amides and 2-aminobenzothiazole were tested in vitro against *Mt*SK to characterize their modes of inhibition by LC-MS. Other orthogonal assays were utilized as confirmatory tool, including proton nuclear magnetic resonance spectroscopy (^{1}H-NMR), dynamic light scattering (DLS), transmission electronic microscopy (TEM), and centrifugation assays to determine the solubility of the compounds and particle size of the aggregates. The possibility of these compounds to inhibit *Mt*SK through aggregation based mechanism of action and traverse through *Mtb* cell wall was predicted by the use of aggregate advisor tool and MycPermCheck tool, respectively.

2.2 Materials and methods

2.2.1 Chemicals

All fourteen synthetic compounds containing oxadiazole-amide and 2-aminobenzothiazole scaffolds used on this study were supplied by Life Chemicals with a minimum purity of 90% as analyzed by NMR. Water and acetonitrile solvents were LC/MS grade and were purchased from Thermo Fisher (Atlanta, GA). All buffers and media were prepared using water purified by a Milli-Q purification system (Millipore, Billerica, MA). *Mt*SK was expressed and purified following procedures described by Simithy et al [61]. The purity of the protein after Ni^{2+} affinity chromatography was determined by SDS-PAGE and LC-ESI-Q-TOF-MS, and aliquots were stored at −80 °C in 50 mM Tris-HCl, pH 7.4; 0.5 M NaCl. Detergent Triton X-100, shikimic acid, adenosine-5'-triphosphate (ATP) ammonium acetate, dimethyl sulfoxide (DMSO), dimethyl sulfoxide-d6 (DMSO-d6) (D,99.96%), deuterium oxide (D_2O) (D,99.99%), KH_2O_4, KCl, $MgCl_2$, NaCl, Tris-HCl and formic acid were bought from Sigma-Aldrich (St. Louis, MO, USA). Shikimate-3-phosphate (S3P) with a minimum purity of 90% for the calibration curve was

purchased from Santa Cruz Biotechnology, Inc (Dallas, TX). TMSP-2,2,3,3-D4 (D,98%) sodium-3-trimethylsilylpropionate was bought from Cambridge Isotope Laboratories, Inc.

2.2.2 Non-specific binding determination to *Mt*SK by LC-MS functional assay

From the list of the 14 compounds, compounds **3**, **4**, **7**, and **14** with the lowest IC$_{50}$, 3.79, 10.35, 3.43, and 1.94 µM, respectively were selected to be tested in the LC-MS functional assay [49]. All compounds were tested each at 100 µM against *Mt*SK at 200 nM. The same compounds were retested against *Mt*SK at 20 nM to investigate inhibitory activity difference from the 200 nM. An LC-MS approach was used to assess the extent of inhibition by monitoring the production of S3P during the reaction catalyzed by *Mt*SK.

Accordingly, test compounds were dissolved in DMSO and pre-incubated with *Mt*SK at 25 °C for 30 minutes in a microcentrifuge tube containing ammonium acetate buffer 100 mM, pH=7.6, KCl 50 mM and MgCl$_2$ 5 mM in a 500 µL reaction volume at 25 ºC. The enzymatic reaction was commenced by the addition of 5 mM shikimic acid, and 1.2 mM ATP for 30 seconds, quenched by the addition of 2 µL of 98% formic acid and injected into LC-MS. DSMO was added as a negative control instead of the test compounds [61]. The DMSO concentration was always ≤ 2% (v/v) in the experiments, which was observed not to affect the results. The same assay as described above was carried out with some modifications by adding a detergent 0.01% v/v Triton X-100 in the presence and absence of the test compound to monitor non-specific inhibition (Fig. 2.1). For reproducibility purposes, all functional assays were conducted in duplicate and analyzed twice. All compounds were evaluated for percentage of inhibition against *Mt*SK at 200 and 20 nM by using Eq. (1) [68]

$$(1) \ \%Mt\text{SK Inhibition}=100 \ (c0-c) \ c0$$

where c0 depicts the S3P peak area observed in the absence of an inhibitor (control experiments) and c depicts the peak observed in the presence of test compounds.

2.2.2.1 LC-MS analysis and quantification of S3P in the *Mt*SK functional assay

Reversed-phase HPLC separation of the reaction mixtures was performed on an Agilent 1200 RRLC system, using a Zorbax Eclipse Plus Phenyl-hexyl (4.6 x 100 mm 3.5 μm, Agilent Technologies, Inc.) column. The mobile phase consisted of water with 0.1% (v/v) formic acid (A) and acetonitrile 100% (B) with a gradient elution as follows: 0 min, 2% B held for 4 min, to 30% B in the next 2 min. Each run was followed by a 1 min post-run with 2% B. The total run-time analysis was 7 min at a flow rate of 0.4 mL/min and column temperature of 45 °C.

Mass spectrometry was carried out in an Agilent (Little Falls, DE) 6520 Accurate-Mass Q-TOF. All acquisitions were performed under electrospray ionization (ESI), in the negative ionization mode, using selected ion monitoring (SIM) and a narrow *m/z* range (*m/z* 100-300). A capillary voltage of 3200 V was used for the ESI source, nitrogen was used as the nebulizing gas (25 psig) and drying gas (10 L/h, 350 °C) and the fragmentor voltage was set to 175 eV. For quantification of S3P, extracted ion chromatograms (EIC) of *m/z* 253.0117 [M-H]⁻ were integrated using Agilent MassHunter Workstation Qualitative Analysis software (version B.02.00), and the peak area was used to evaluate enzyme activity. For quantification of S3P, extracted ion chromatograms (EIC) of *m/z* 253.0117 [M - H]⁻ of control and inhibitor samples were integrated using Agilent MassHunter Workstation Qualitative Analysis software (version B.02.00), and the peak areas were used to evaluate enzyme activity.
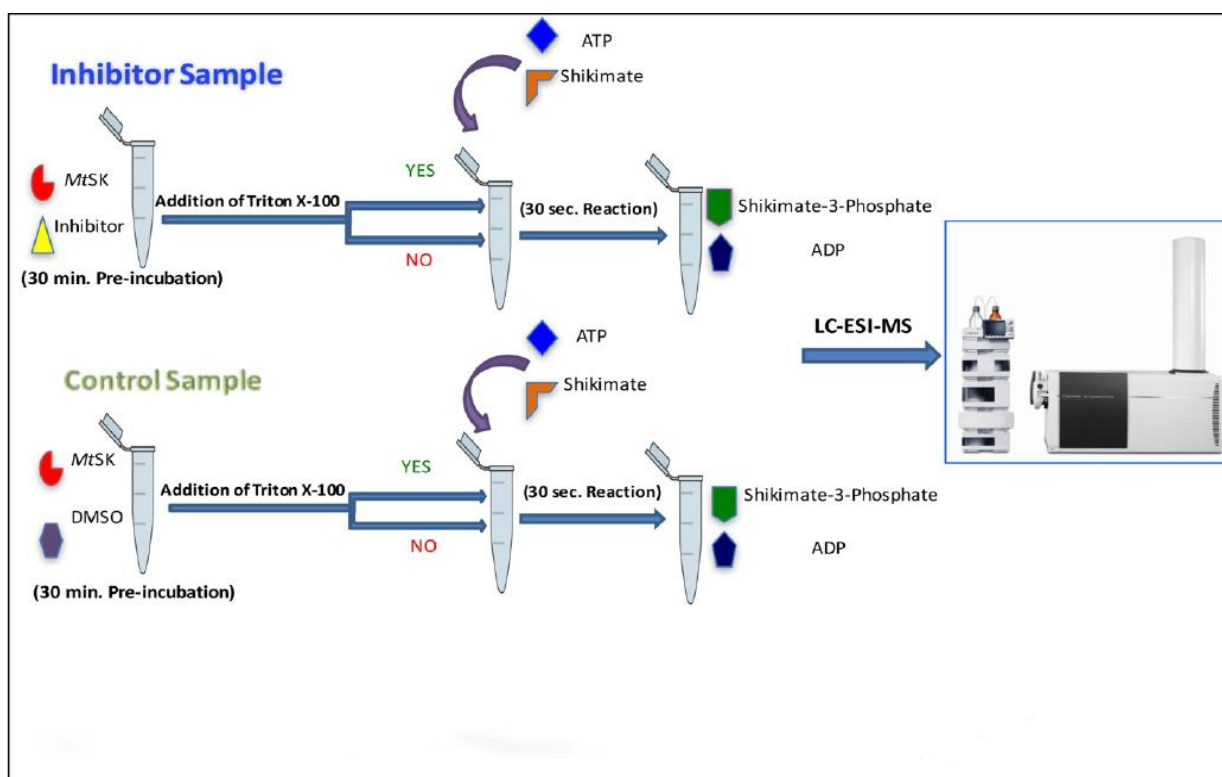
Figure 2.1. Schematic representation of *Mt*SK detergent-based assay by LC-MS.

2.2.2.2 Construction of shikimate-3-phosphate calibration curve.

S3P as an external standard was dissolved separately in water to prepare a 1mg/mL stock solution then diluted to obtain a series of stock concentrations according to dilution factor 1:1.5:2. For calibration curve construction, a series of dilutions of S3P were made by diluting the stock solutions of S3P reference standard with water in the presence of 5 mM shikimic acid, 1.2 mM ATP, and 2 μL of 98% formic acid to yield working solutions with concentrations of 2.31, 3.47, 6.94, 10.41, 20.83, 31.25, 62.50, 93.74 μg/mL. Each working solution was analyzed by LC-ESI-MS. A blank sample (average) response was subtracted from each measured standard to obtain the corrected value. The calibration curve points were obtained by using least squares regression analysis. The analysis was conducted in triplicate.

2.2.2.3 Determination of concentration-response curves

The concentration-dependent effects of compounds **3,4,7**, and **14** were scrutinized for their IC_{50}, curve shape, and Hill slope value to determine specific or non-specific inhibitions. All compounds were dissolved in dimethyl sulfoxide (DMSO) and diluted serially to deliver concentrations ranging from 0.781 µM to 200 µM against 20 nM of *Mt*SK and injected into LC-MS as described above in Section 2.2.2. Nonlinear concentration response curves were plotted using log inhibitor concentration against *Mt*SK inhibition percentage, using GraphPad Prism 5.04 (Mountain View, CA) yielding IC_{50} values.

2.2.3 Confirmatory tests for non-specific binding to *Mt*SK

2.2.3.1 Determination of solubility by ^{1}H-NMR spectroscopy

Compound **9** containing an oxadiazole-amide ring (Fig. 2.2), with cLogP value of 2.703 was used for solubility evaluation assay, utilizing a modified method developed by Sittiwong et al [65]. Compound **9** (1.2 mg), was dissolved in 1 mL DMSO-D_6 and serially diluted to deliver different stock concentrations. Stock solutions were used to obtain variable final concentrations of 0.781, 1.56, 3.125, 6.25, 12.5, 25, 50, 100, and 200 µM for NMR assay. All NMR samples consisted of 50 mM potassium phosphate buffer at pH 7.2 (uncorrected) and 50 mM of 3-(trimethylsilyl) propionic2,2,3,3-d$_4$ acid sodium salt (TMSP-D$_4$) were dissolved in 570 µL D$_2$O and 30 µL (5%) of the compound stock. The total volume of the mixture solution was 600 µL. The buffer and DMSO concentrations were fixed for all NMR samples; only the compound concentration changed. A sample containing 600 µL of the mixture in a 5 mm NMR tube was analyzed by NMR spectroscopy. 1D ^{1}H NMR tool was used to assess concentration dependent micelle formation (peak broadening).

2.2.3.1.1 ^{1}H-NMR spectroscopy analysis

A Bruker Avance II NMR 600-MHz spectrometer equipped with a 5 mm triple-resonance cryoplatform (Bruker Biospin, Billerica, MA) with a z-axis gradient operating at ^{1}H NMR experiments. All spectra were acquired at room temperature, 128 scans, 0 dummy scans with total time of 33.333 minutes. The NMR spectra were processed and analyzed using Bruker TopSpin 3.5.
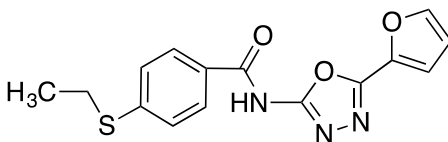

Figure 2.2. Structure of compound 9 containing oxadiazole-amide scaffold.

2.2.3.2 Determination of particle size of aggregates

2.2.3.2.1 Calculations of cLogP and solubility

Predicted properties and descriptors including cLogP and solubility of the fourteen compounds were computed using in silico software, the QikProp suite as implemented in the Schrödinger software package (QikProp, version 4.4, Schrödinger, LLC, New York, NY, 2015).

2.2.3.2.2 Measurement by dynamic light scattering (DLS)

All test compounds were dissolved in DMSO, and diluted in either a filtered ammonium acetate buffer or deionized water at pH 7.6, and 7, respectively to deliver a final concentration of 100 μM in the presence and absence of 0.01% v/v Triton X-100.

A volume of 10 μL of 0.01% Triton X-100 was added to the buffer prior to the addition of the compounds. All samples were allowed to stand at room temperature for 30 minutes and analyzed for particle size by Direct Light Scattering Instrument Particle Sizer NICOMP[TM] 380 ZLS instrument. Three replicates were prepared for each sample (Fig. 2.3) [29,67].
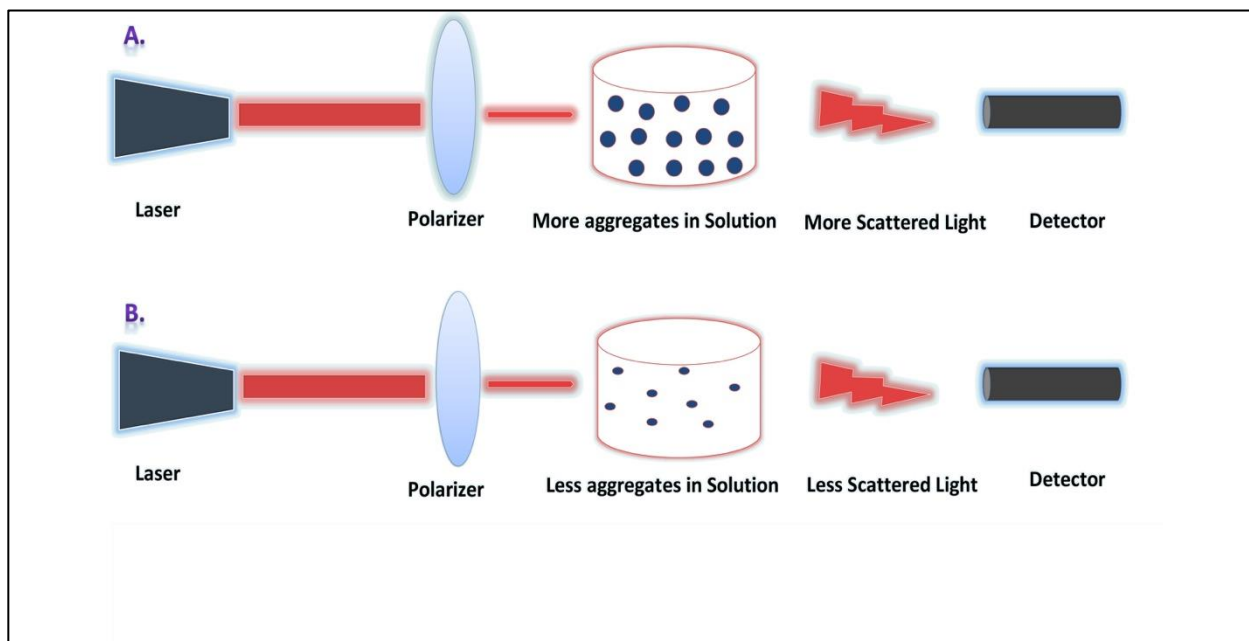
Figure 2.3. Schematic representation of dynamic light scattering assay (DLS). A. More aggregate formation of the compound in absence of the detergent (Triton X-100). B. Less aggregate formation of the compound in presence of the detergent (Triton X-100).

2.2.3.2.3 Measurement by transmission electronic microscopy (TEM)

Solutions of compound **14** at 100 μM with and without 0.01% v/v Triton X-100 and *Mt*SK were prepared in 100 mM ammonium acetate, pH 7.6, at room temperature. A volume of 3 μL from each sample was added to a carbon-coated grid and negatively stained with 1% phosphotungstic acid (PTA). Filter paper was used to absorb excess solution of the sample in the grid that was not required in the examination. Images were obtained with a Zeiss EM 10 Transmission Electron Microscope (TEM). Micrographs were recorded at 25-80 K magnification (Fig. 2.4) [67].
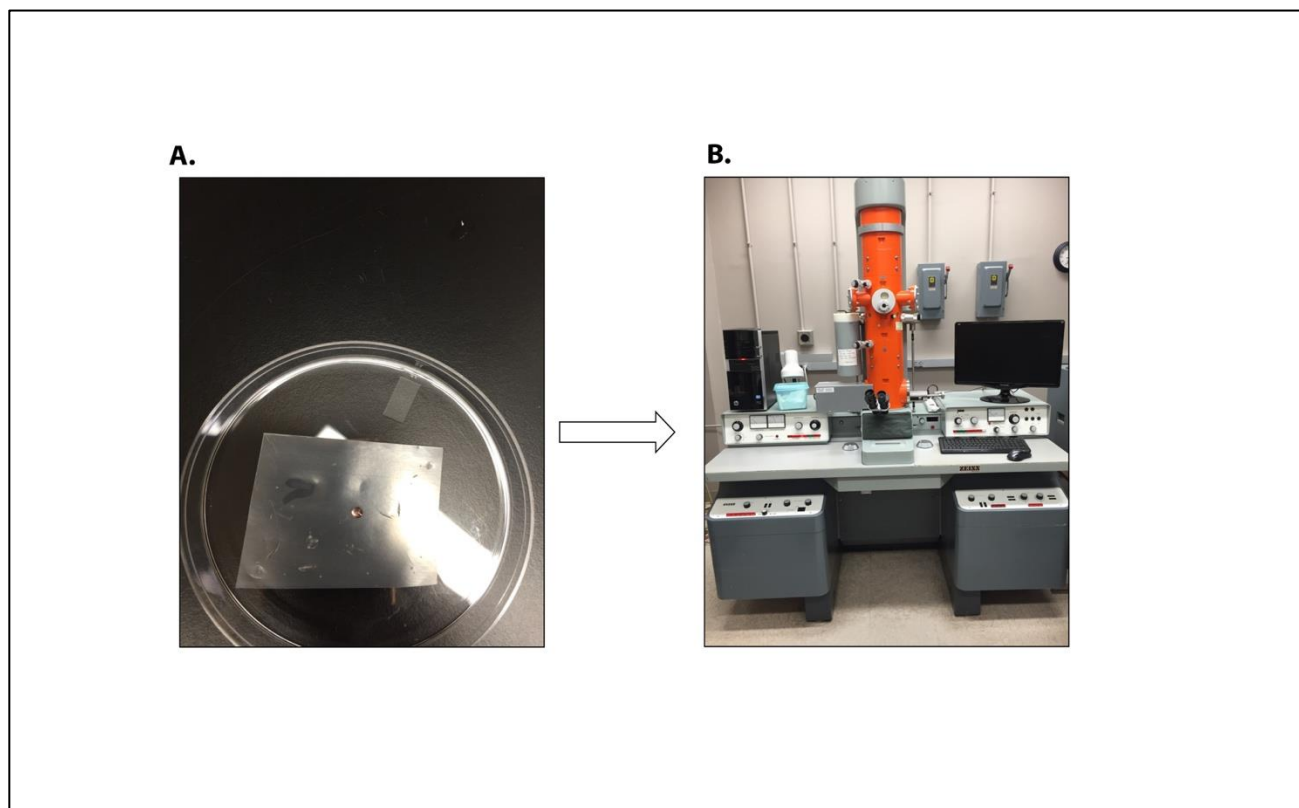
Figure 2.4. Sample examination under transmission electronic microscopy (TEM).
A. Carbon-coated grid where samples were placed to be examined under TEM. B. Zeiss EM 10 transmission electron microscope (TEM).

2.2.3.3 Visualization of precipitate formation

All compounds were dissolved in DMSO at 1mg/mL, then diluted to deliver 100 µM and 50 µM in a microcentrifuge tube containing ammonium acetate buffer 100mM, pH 7.6, KCl 50 mM and $MgCl_2$ 5 mM in a total volume of 500 µL. Consequently, test compounds were visually examined and centrifuged at $14000 \times g$ for 40 minutes at 4 °C to inspect for pellet formation [70].

2.2.3.4 Aggregate formation prediction by aggregate advisor tool

An aggregator advisor tool developed by Shoichet Laboratory at UCSF (http://advisor.bkslab.org) was utilized to identify compounds that have the tendency to form aggregates and produce false positive in bioassays. It also suggests alternative approaches to proving whether these results are artifacts or not [64]. In the aggregator advisor tool, all fourteen

compounds were converted into their SMILES strings and pasted into a text box, or structurally drawn into a drawing box, then submitted. A report was generated for each compound containing its LogP value, and the likelihood in percentage of the compound to be similar to a compound structure previously known to form an aggregation.

2.2.4 *Mtb* cell wall permeability prediction by MycPermCheck tool

Mtb permeability prediction tool (MycPermCheck) was developed by Merget et al. (http://mycpermcheck.aksotriffer.pharmazie.uni-wuerzburg.de/) which helps to estimate the penetration probability of small organic compounds through mycobacterial cell wall and it is only applicable to small molecules, with a molecular weight not above 500 Dalton [66]. The computational tool was employed to predict the permeability of the fourteen compounds across *M. tuberculosis* cell wall without considering uptake mechanisms.

Chapter 3: Results and discussion of the characterization of *M. tuberculosis* shikimate kinase inhibitors containing oxadiazole-amide and aminobenzothiazole rings by using LC-MS and other orthogonal confirmatory assays.

3.1 Non-specific inhibition of *Mt*SK by oxadiazole-amide and 2-aminobenzothiazole

Compounds **3**, **4**, **7**, **11**, **12**, **13**, and **14** were screened for non-specific inhibition against 200 nM and 20 nM *Mt*SK at 100 µM in the absence and presence of 0.01% v/v Triton X-100 by utilizing LC-MS-based functional assay as described in Section 2.2.2. Negative control experiments were conducted in a similar way but in the absence of both, test compounds and Triton X-100. Fig. 3.1 shows an overlaid chromatogram of three peak areas of shikimate-3-phosphate (S3P) product, the peak area of S3P was significantly reduced in the presence of the compounds only, indicating inhibition of *Mt*SK. On the other hand, the peak area of S3P was slightly decreased in the presence of the compound and 0.01% v/v Triton X-100, suggesting disruption of aggregates formed by the compounds. Negative control (in the absence of test compound and 0.01% v/v Triton X-100) displayed the highest S3P peak area. Initially, in the absence of 0.01% v/v Triton X-100, at 20 nM of *Mt*SK, test compounds including, **3**, **4**, **7**, and **14** showed > 80 % *Mt*SK inhibition and compounds **11**, **12**, **13** displayed > 30 % *Mt*SK inhibition (Table 3.1). Conversely, the extent of inhibition of the compounds mentioned above was reduced, when the concentration of *Mt*SK was increased 10-fold, from 20 nM to 200 nM (Table 3.1), a concentration that was found to provide an optimum kinetic parameter (K_{cat}) of *Mt*SK [61]. This finding correlates with the premise that non-specific inhibitors by aggregation were attenuated largely by the increase of an enzyme concentration [36, 69].

To further study if the aggregates could be broken down by the use of a detergent, briefly, two detergents were evaluated, 0.01% v/v Triton X-100 and 0.00004% v/v Tween-80 in control

experiments. The inclusion of 0.00004% v/v Tween-80 reduced catalytic activity of MtSK (data not shown). However, the addition of 0.01% v/v Triton X-100 did not affect K_{cat} of MtSK (data not shown); therefore, 0.01% v/v Triton X-100 was used in this study. We conducted the same method as described above in the presence of 0.01% v/v Triton X-100, compounds **3**, **4**, **7**, **11**, **12**, **13**, and **14** at 100 µM were assayed against 20 nM and 200 nM MtSK. Inhibition percentages were substantially reduced by $\geq$ 1-fold and the activity of MtSK was retained (Table 3.1), indicating that the inhibition mechanism was reversible and non-specific binding. A phenomenon that was also observed by McGovern et al [67].
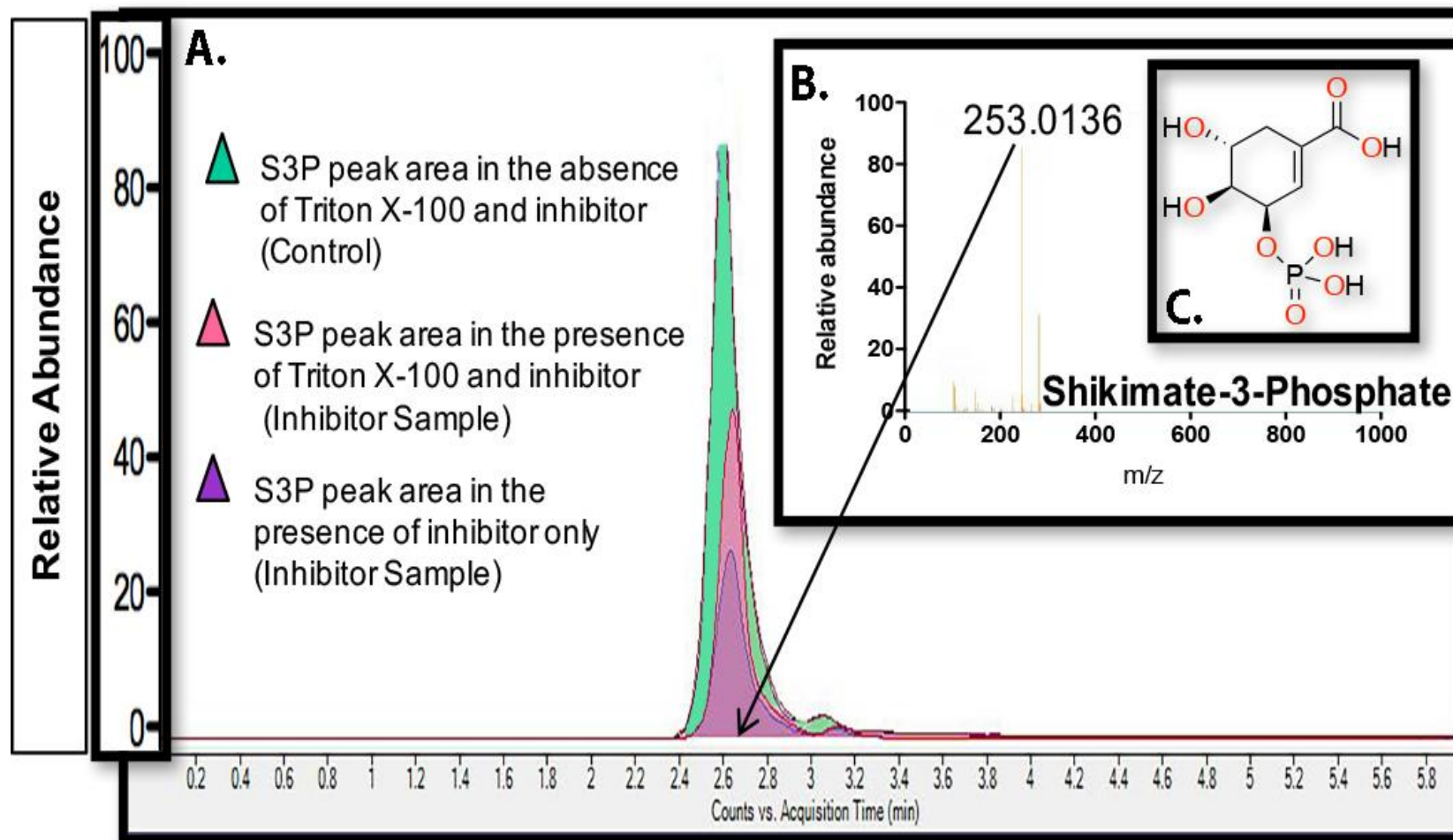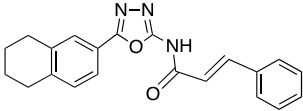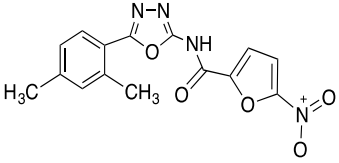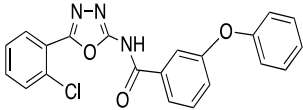
Figure 3.1. A. An extracted ion chromatogram of shikimate-3-phosphate in different conditions. B. ESI-MS spectrum showing shikimate-3-phosphate (S3P) ionic mass. C. Chemical Structure of shikimate-3-phosphate (S3P) .

Table 3.1. Effect of 0.01% Triton X-100 on *Mt*SK inhibition by oxadiazole-amide and aminobenzothiazole at 100 μM.

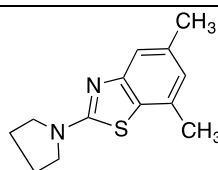|		20 nM *Mt*SK		200 nM *Mt*SK	
		Without Triton X-100	With Triton X-100	Without Triton X-100	With Triton X-100
Structure	Class	Inhibition %		Inhibition %	
3	Oxadiazole-amide	98	33.8	31.17	12
4	Oxadiazole-amide	96	19	46	38
7	Oxadiazole-amide	83	11	32	9
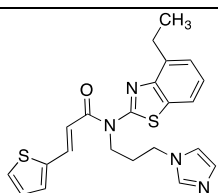
11	Aminobenzothiazole	55	44	38	13
12	Aminobenzothiazole	37	32	16	6.5
13	Aminobenzothiazole	55	34	8	5
14	Aminobenzothiazole	90	57	37	14
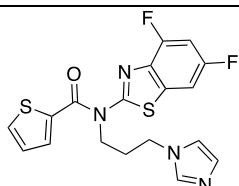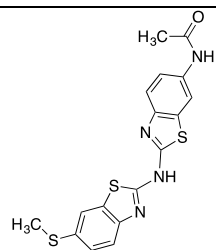
3.1.1 Evaluation of concentration-response curves

Although the results described in 2.3.1 are reasonably reliable indicating aggregation based mechanism of action, we decided to perform concentration-response curves experiments to evaluate IC_{50} values, curve shape, and Hill slope. We selected the most active compounds **3**, **4**, **7**, and **14** from the set [49]. According to a dilution factor 1:2, concentrations ranging from 0.781-200 μM were tested against 20 nM of *Mt*SK at room temperature followed by LC-MS analysis. IC_{50} values were determined by comparing the S3P produced in the presence of nine concentrations of each compound with the S3P produced in the negative control samples (No inhibitor). Percentage of *Mt*SK inhibition was determined using the following equation: $100(c0 - c)/c0$, where c0 was the amount of S3P formed in the absence of the inhibitor and c was the S3P formed in the presence of the inhibitor. Fig. 3.2 shows concentration-response curves for compounds **3**, **4**, **7**, and **14**. All compounds displayed curve steepness, Hill coefficient >1, and the difference in % inhibition occurred over a narrower range of inhibitor concentration, which is a common pattern among non-specific inhibitors. However, a classical, one to one binding inhibition occurs gradually, over a wider range of inhibitor concentrations [27]. The values of IC_{50} of compounds **3**, **4**, **7**, and **14** that were tested against 20 nM *Mt*SK, were 22.49, 15.22, 27.81, and 19.03 μM, respectively, which were higher than the ones that were determined previously (Table 3.2) in our laboratory by Simithy et al [49]. The IC_{50} difference in both studies are in good agreement with the presumption, that the increase of an enzyme concentration increases the IC_{50} of compounds that display non-specific inhibition by aggregation [36,69]. Last but not least, we visually inspected concentration-response curve of compound **3,** which was determined by Simithy et al [49]. Intriguingly, it was somehow similar to the concentration-response curve of compound **3** determined in this study. Both had a situation where there was an abrupt reduction of inhibition.
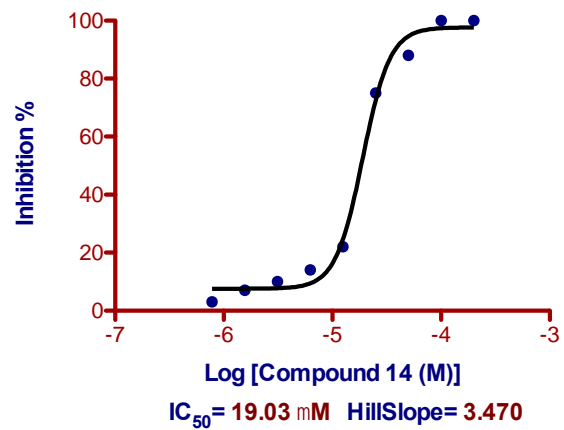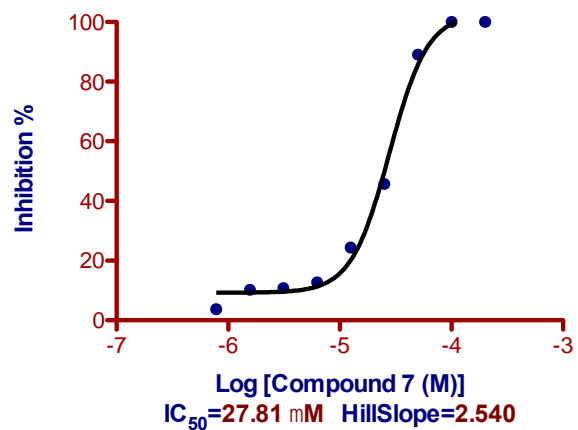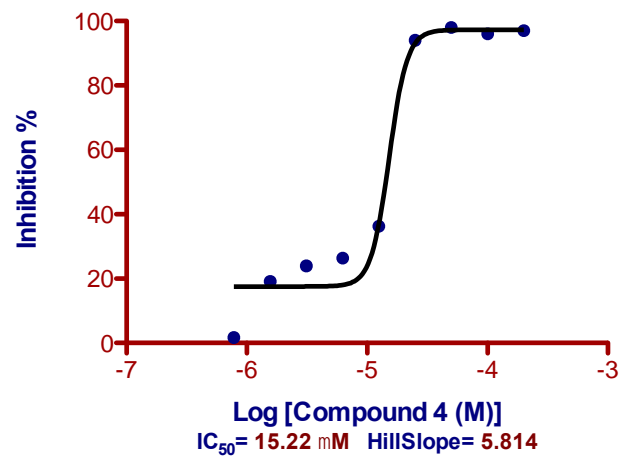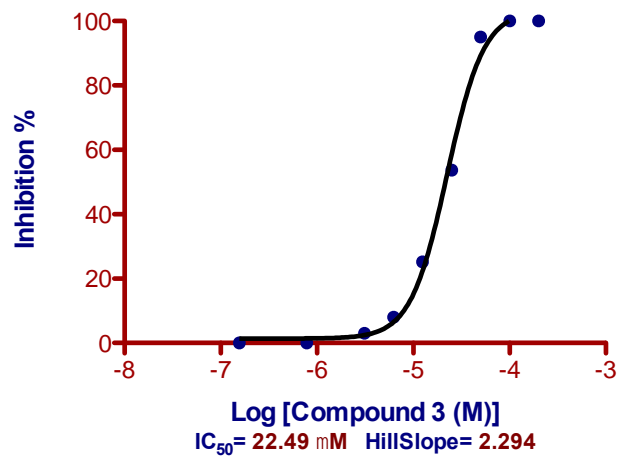
Figure 3.2. Concentration response-curves values of compounds 3, 4, 7, and 14. All show curve steepness and high Hill Slope > 1.

Table 3.2. IC$_{50}$ values of non-specific inhibitors against 20 nM and 15 nM purified *Mt*SK.

Compound no	IC$_{50}$ (µM) [*] *Mt*SK 20 nM	IC$_{50}$ (µM) [**] *Mt*SK 15 nM
3	22.49	3.79
4	15.22	10.35
7	27.81	3.43
14	19.03	1.94

[*]Values reported in this study.   [**]Values reported by Simithy et al [49].

3.2 Confirmation of non-specific inhibition of *Mt*SK

3.2.1 Micelle formation determination by ^{1}H-NMR spectroscopy

^{1}H NMR spectroscopy was utilized, to monitor peak broadening of ^{1}H NMR spectra as a function of compound concentration due to micelle formation. Compound **9** was selected because it was the most soluble compound among the list with a solubility value of -4.246 ^{1}H NMR spectra of compound **9** was analyzed at different concentrations 0.781, 1.56, 3.125, 6.25, 12.5, 25, 50, 100, and 200 µM. Fig. 3.4 displays ^{1}H NMR spectra of compound **9**, peak broadening was observed from 6.25 µM up to 200 µM, which indicates aggregate formation. Peak broadening at 200 µM was prominent, and a gradual reduction of peak broadening was observed at lower concentrations. In contrast, a non-aggregator, Pranlukast, a leukotriene receptor-1 antagonist, which is used to treat asthma showed no peak broadening [71].

Since the value of IC$_{50}$ of compound **9** was previously determined in our laboratory and reported as 20.73 µM by Simithy et al [49]. ^{1}H NMR spectra of compound **9** in Fig. 3.4 showed peak broadening (aggregation) even at 6.25 µM, which indicates that compound **9** showed non-specific inhibition against *Mt*SK by aggregate formation.

The protons that were attached to the methyl and ethyl groups present in the aliphatic side chain shown in Fig. 3.3 were selected to monitor peak broadening because they were easily recognized and differentiated in ^{1}H NMR spectra. Moreover, the aliphatic portion of the compound influences the extent of lipophilicity, which results in lower solubility and aggregate formation of the compound in the buffer solution.
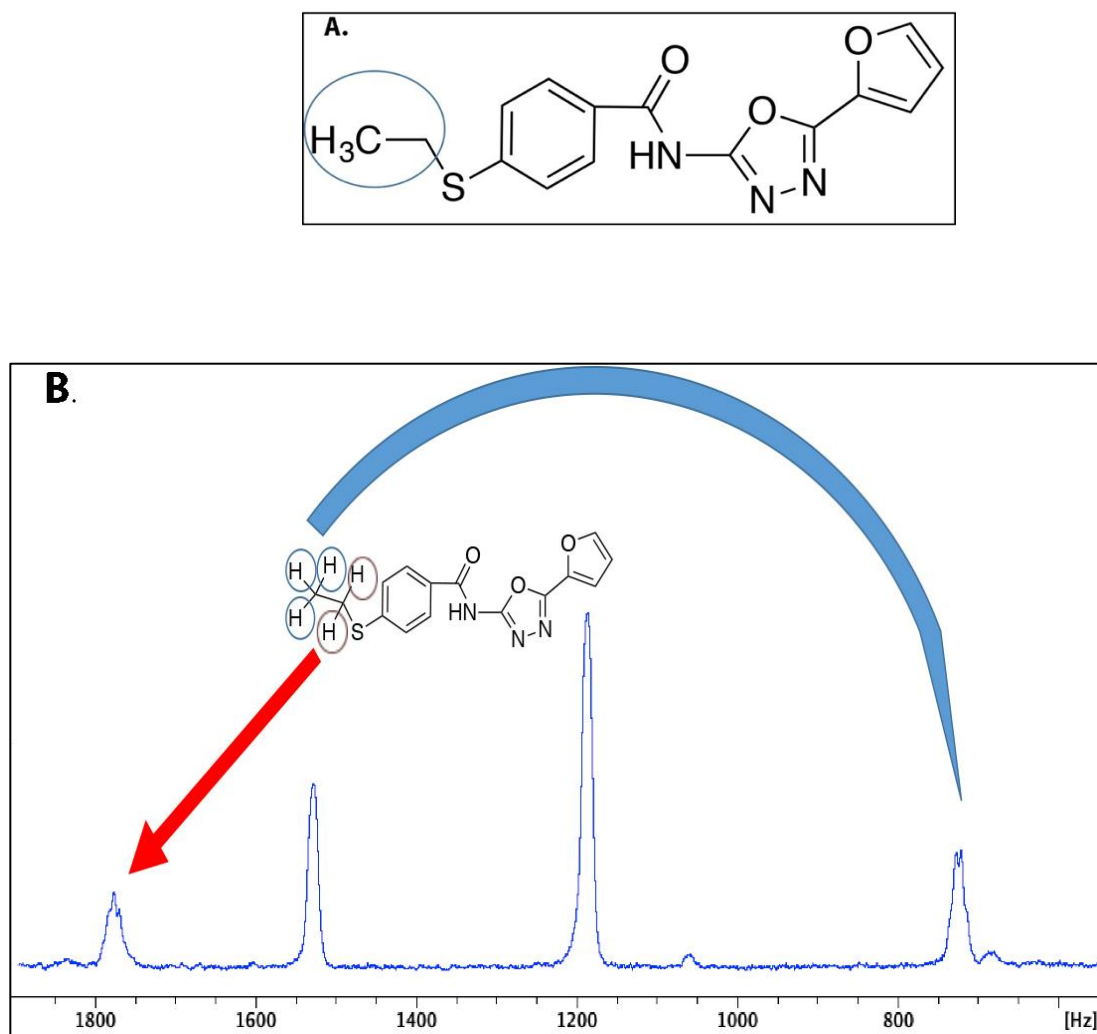

Figure 3.3. ^{1}H NMR spectrum of selected protons of compound 9 to be monitored for micelle formation. A. Structure of compound 9, circled protons in the aliphatic portion were selected to monitor evidence of peak broadening on ^{1}H NMR spectrum. B. Circled protons of methyl group represent a doublet signal with a chemical shift at 721.6 Hz (Upfield), circled protons of ethyl group represent a quartet signal with a chemical shift at 1776.0 Hz (Downfield).
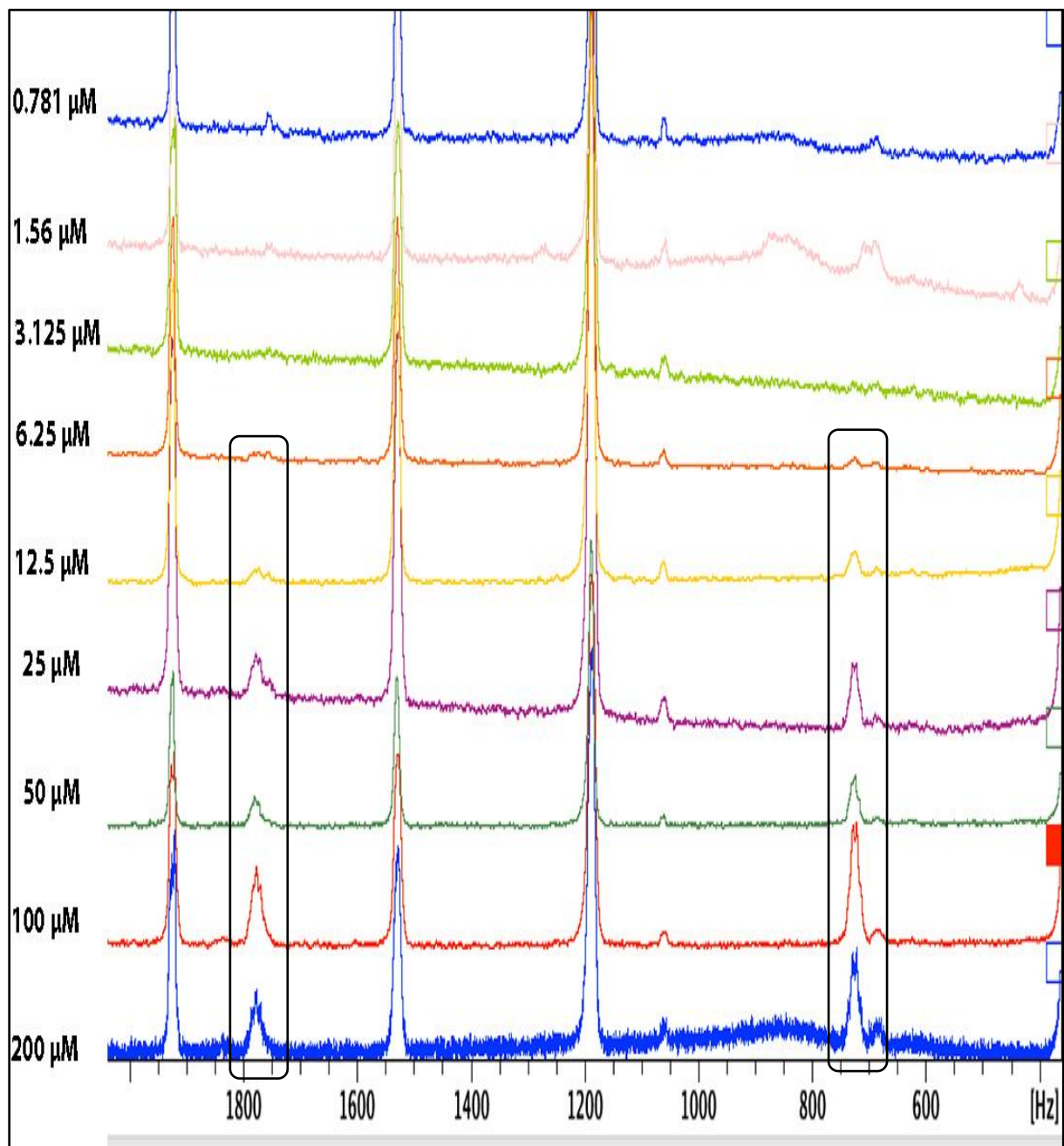
Figure 3.4. ^{1}H NMR spectra of compound 9 producing micelle formation (peak broadening) from 200 μM down to 6.25 μM.
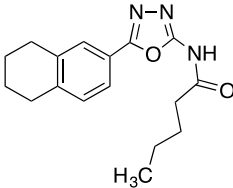
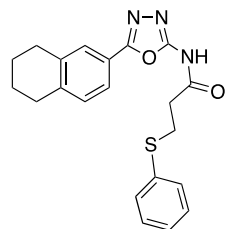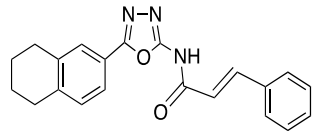**3.2.2 Assessment of particle size of aggregates**

**3.2.2.1 Analysis of dynamic light scattering (DLS) data**

Dynamic light scattering (DLS) is a popular technique in polymer and particle sciences to determine the size and distribution of particles in solutions. It can be used in many applications to determine particle sizes in solutions, including emulsions, micelles, polymers, proteins, nanoparticles or colloids. In this study, the dynamic light scattering instrument was used as a complimentary tool to confirm non-specific inhibition by aggregate formation. The results in this study were assessed based on two parameters, scattering intensity and average particle size, which were measured based on the autocorrelation functions of the scattered laser light. Compounds **1**, **2**, **3**, **4**, **5**, **6**, **7**, **8**, **9**, **10**, **11**, **12**, **13**, and **14** at 50 and 100 µM were dissolved in two media, ammonium acetate buffer and water, in which they displayed high light scattering intensity and particle size suggesting aggregation. On the other hand, when 0.01% Triton X-100 was added to the compounds, they showed low light scattering intensity and particle size, indicating dissolution of aggregates formed by the compounds. Table 3.3 shows results of test compounds at 50 µM in ammonium acetate buffer. In the absence of 0.01% Triton X-100, compounds displayed an average scattering intensity and particle size of 252 k count 1479 nm, respectively, whereas in the presence of 0.01% Triton X-100, showed an average scattering intensity of 106 k count and 211 nm, respectively. The effect of 0.01% Triton X-100 was evident on the aggregates, which resulted in > 1-fold reduction of the average scattering intensity and 6-folds decrease in particle size.

In the absence of 0.01% Triton X-100, test compounds at 100 µM, showed an average scattering intensity of 292 k count and particle size of 1731 nm, while in the presence 0.01% Triton X-100, they displayed an average scattering intensity of 136 k count and particle size of 343 nm. The average scattering intensity and particle size were reduced by > 1-fold and 5-folds, respectively, in the presence of Triton X-100. Table 3.4 exhibits results of test compounds at 50

µM water instead of ammonium acetate in the absence of 0.01% Triton X-100, displayed an average scattering intensity and particle size of 244 k count 1431 nm, respectively whereas in the presence of 0.01% Triton X-100, they showed an average scattering intensity of 103 k count and 206 nm, respectively. The average scattering intensity and particle size were reduced by > 1-fold and 6-folds, respectively, in the presence of Triton X-100. Test compounds at 100 µM, in the absence of 0.01% Triton X-100, compounds showed an average scattering intensity and particle size of 280 k count and 1680 nm, respectively while in the presence of 0.01% Triton X-100, they displayed an average scattering intensity and particle size of 126 k count and 328 nm, respectively. The average scattering intensity and particle size were reduced by > 1-fold and > 4-folds, respectively, in the presence of Triton X-100. For all of these compounds in both media, the difference in scattering intensity with and without the detergent strongly suggest that these compounds formed aggregates in the buffer solution and were disrupted by the effect of the detergent.
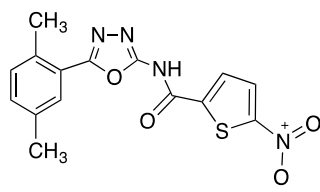
Table 3.3. Scattering intensities and average particle sizes of test compounds with significant DLS signals in ammonium acetate pH 7.6.

| Compound Concentration	50 μM				100 μM			
	Without Triton X-100		With Triton X-100		Without Triton X-100		With Triton X-100	
Structure	Intensity (k Counts)	Size (nm)	Intensity (k Counts)	Size (nm)	Intensity (k Counts)	Size (nm)	Intensity (k Counts)	Size (nm)
1	228	1317.2	100	167.12	280	1432.4	131	255.2
2	325	1980.4	132	311.45	340	2005.1	158	480.34
3	290	1711.2	110	280	310	1820	141	390
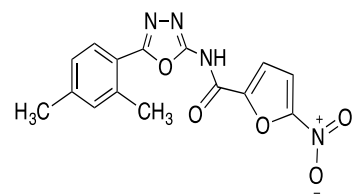
150	613.1	78	118.2	190	851.7	83	131.31

4

195	830.1	85	132.5	240	986.4	85	151.27

5
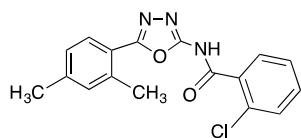
220	1291.7	98	157.5	270	1321.7	115	212.1

6
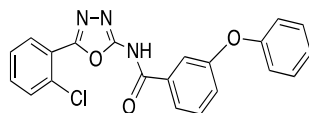
330	2453.2	150	317.4	350	2850.05	180	516.7

7
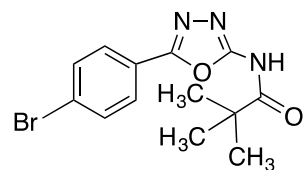
8	205	1151.6	90	140.1	260	1211.11	100	201.5
9	200	900.17	90	139.2	250	1151.71	100	185.41
10	242	1410.3	100	189	300	1620	123	354
11	360	2456.4	220	335.8	400	3776	286	817.2
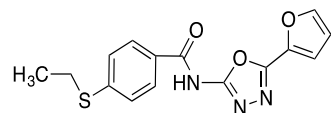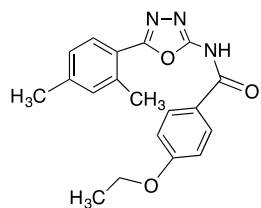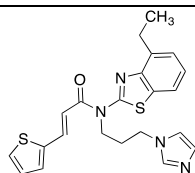
12	252	1512.3	110	190.51	300	1750.2	139	373.1
13	300	1754.62	128	303.5	321	1934	150	470
14	231	1325.7	100	178.11	285	1531.2	122	271.4
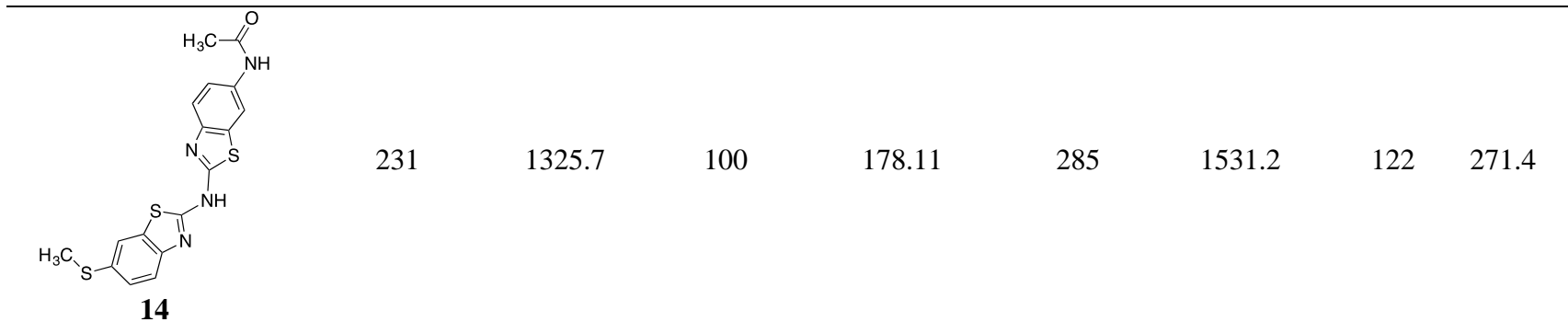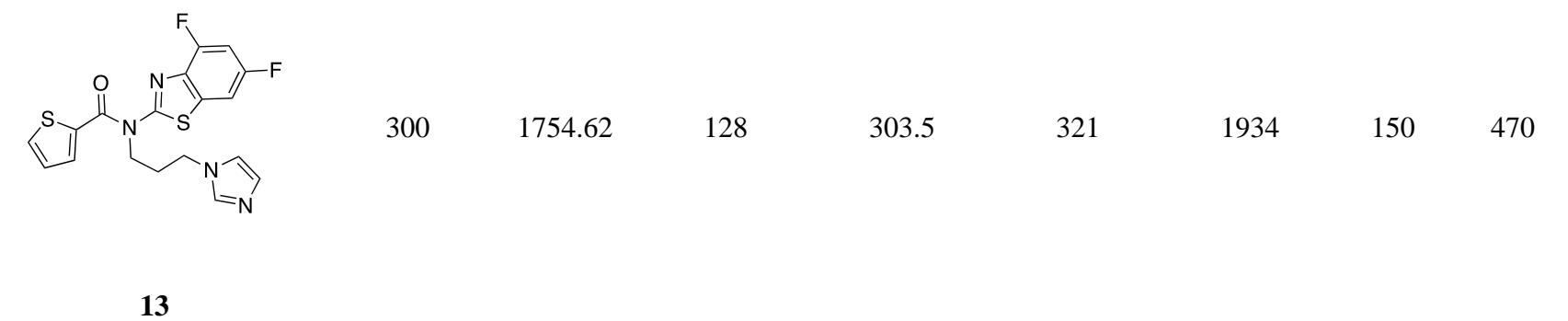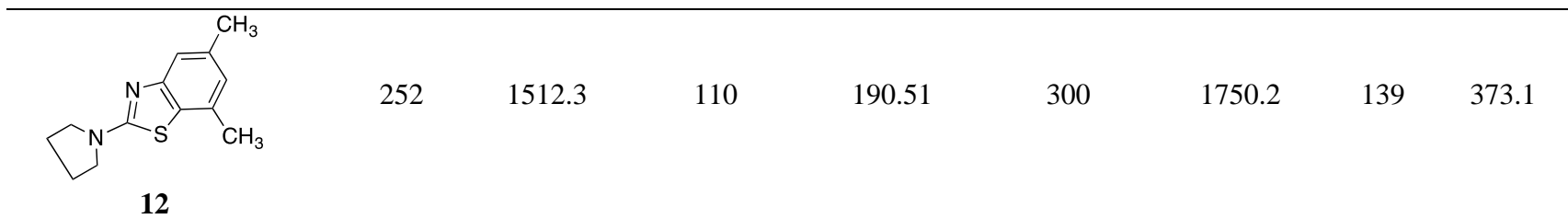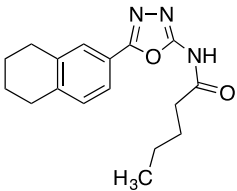
Table 3.4. Scattering intensities and average particle sizes of test compounds with significant DLS signals in water pH 7.

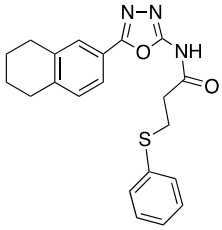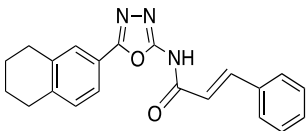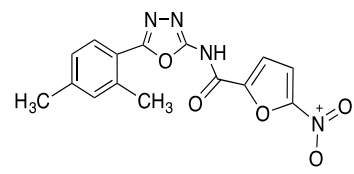| Compound Concentration	50 µM				100 µM			
	Without Triton X-100		With Triton X-100		Without Triton X-100		With Triton X-100	
Structure	Intensity (k Counts)	Size (nm)	Intensity (k Counts)	Size (nm)	Intensity (k Counts)	Size (nm)	Intensity (k Counts)	Size (nm)
1	223	1123.4	83	165.4	260	1324.6	100	259.3
2	280	1911.4	125	305.3	330	1921.1	152	410.34
3	264	1634.5	100	273.4	306	1820.4	138	353.6

Compound								
4	145	738.2	73	123.4	182	823.4	72	131.31
5	192	853.2	75	130.5	237	973.2	80	176.3
6	215	1043.5	80	153.6	255	1301.3	95	203.1
7	340	2331.1	154	320.4	330	2423.2	170	481.6
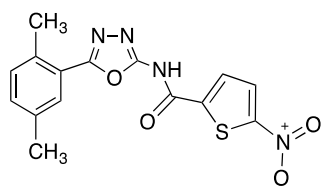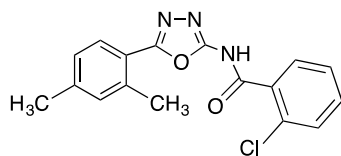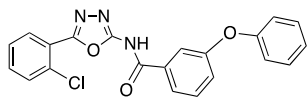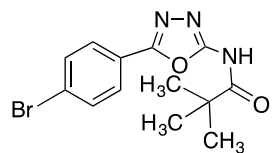
8	210	1031.6	82	143.3	250	1192.3	92	198.5
9	200	890.4	83	138.4	245	1123.1	85	182.5
10	235	1425.3	90	177.4	280	1583.6	122	275.3
11	352	2232.2	200	310	380	3823	270	908
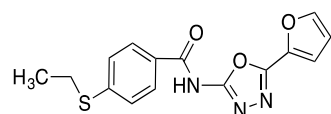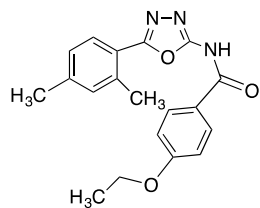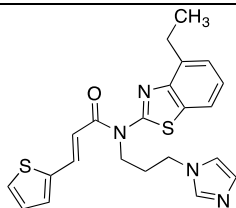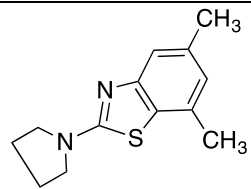
12	250	1546.6	95	185.7	290	1762.6	130	343.7
13	270	1850.62	115	283.4	300	1852.3	143	398.2
14	230	1204.5	90	174.2	270	1438.2	115	275.4
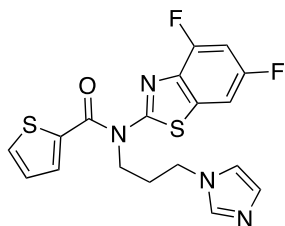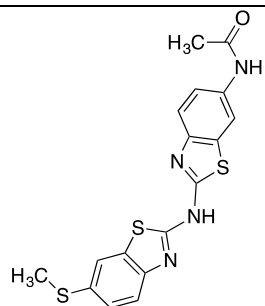
3.2.2.2 Analysis of Transmission electronic microscopy (TEM) data

Transmission electron microscopy (TEM) was used to investigate further if these nonspecific inhibitors form aggregates in aqueous solution since they already have shown to form large particles by DLS. Fig. 3.5 shows images of compound **14** in the presence of 0.01% v/v Triton X-100, in the presence of *Mt*SK, and *Mt*SK alone. In Fig. 3.5-A, aggregates of compound **14** formed large particles with different sizes; these colloidal aggregates are the result of the self-association of the compound molecules in the buffer solution. However, when 0.01% v/v Triton X-100 was added to the compound, the aggregates were disintegrated and resulted in a lower particle size in the submicron range (Fig. 3.5-B). This finding is consistent with what was observed from DLS results. In Fig. 3.5 C, D, and E, images display *Mt*SK alone, buffer crystals in the presence of phosphotungstic acid (PTA) staining solution and compound **14**, and buffer crystals alone, respectively.
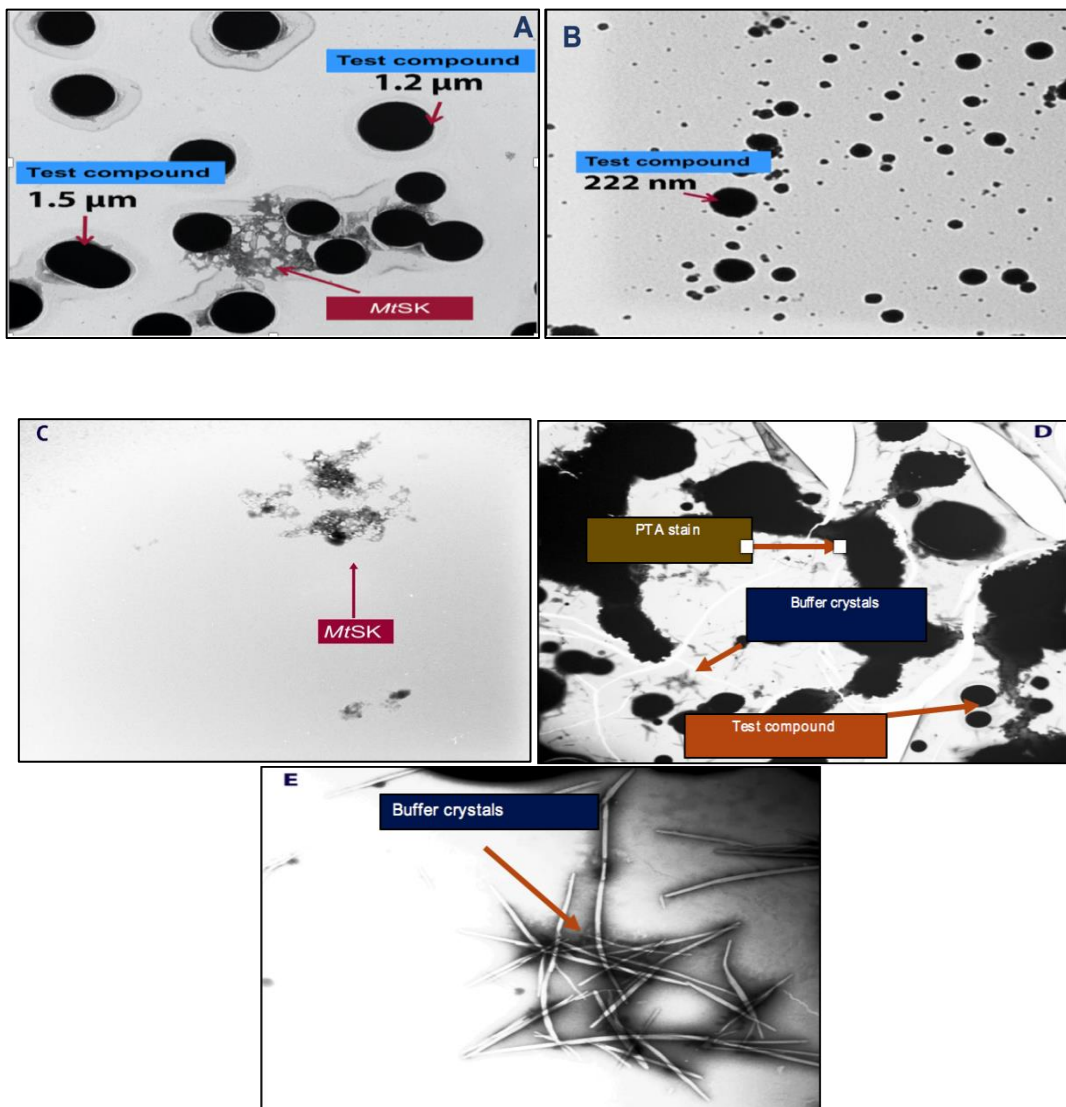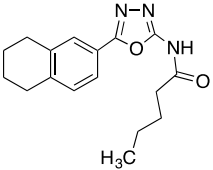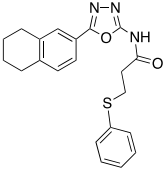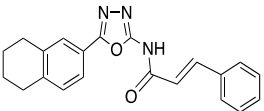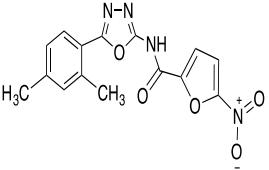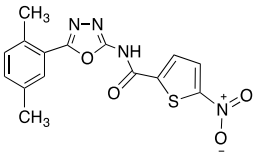
Figure 3.5. Images visualized by transmission electron microscopy: A. Compound 14 in the presence of *Mt*SK. B. Aggregates of compound 14 were disrupted by 0.01% v/v Triton X-100. C. *Mt*SK only in the buffer solution. D. PTA staining solution, buffer crystals and compound 14. E. Buffer crystals only.

3.2.2.3 Calculations of cLogP and solubility

Two parameters were selected, cLogP (partition coefficient) and LogS (solubility) which were computed for the fourteen compounds (Table 3.5). For cLogP calculations, compound **11** was considered the most lipophilic compound from the list with a cLogP of 5.148 whereas compound **4** was the least hydrophobic with a cLogP of 1.736. For solubility prediction, compound **2** was the least soluble compound in aqueous media with a solubility value of -6.854 while compound **9** was the most soluble with a solubility value of -4.246 from the set of the fourteen compounds. Since the results were merely an estimation and not experimentally determined, only cLogP calculations were used because they were in good agreement with the results in dynamic light scattering (DLS) Section 3.2.2.1 and transmission electron microscopy (TEM) Section 3.2.2.2.

Table 3.5. cLogP and solubility values of test compounds calculated with Schrödinger software package

Structure	cLogP	Solubility[*]
1	3.637	-5.193
2	4.306	-6.854
3	4.063	-6.247
4	1.736	-4.329
5	2.206	-4.777
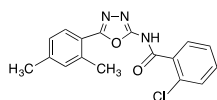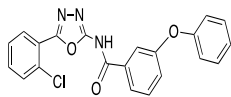
| | 3.553 | -5.466 |
| **6** | | |

| | 4.446 | -6.211 |
| **7** | | |

| | 2.839 | -4.544 |
| **8** | | |

| | 2.703 | -4.246 |
| **9** | | |

| | 3.728 | -5.761 |
| **10** | | |
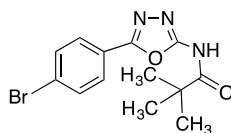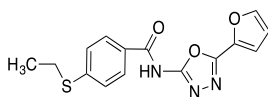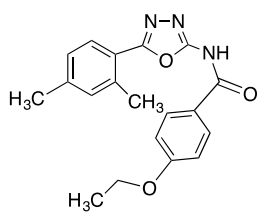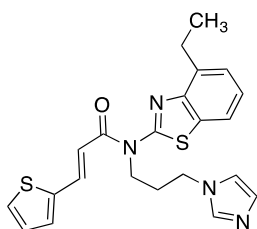
	5.148	-6.02

11
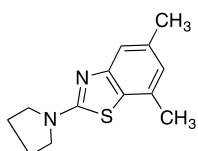
	3.822	-4.688

12
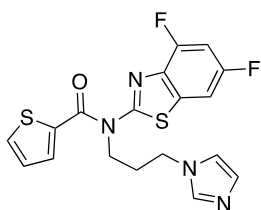
	4.262	-5.003

13
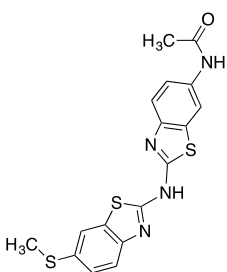
	3.665	-6.102

14

[*]**Predicted aqueous solubility: logS where S is concentration of solute (mol/dm^3) in a saturated solution in equilibrium with crystalline solid. The scale is -6.5 to 0.5 (from least to most soluble)**
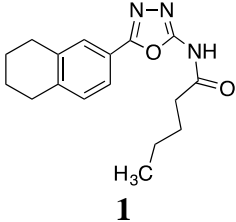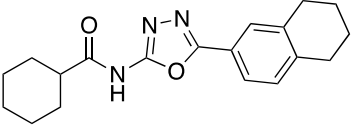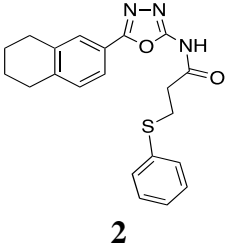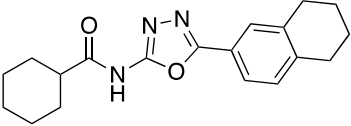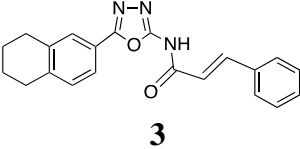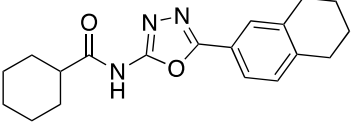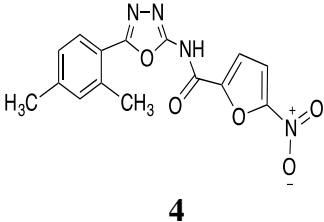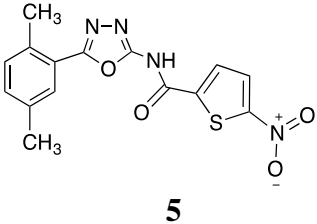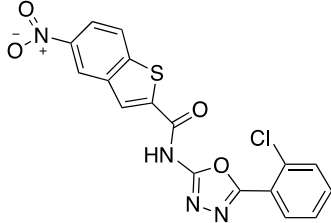
3.2.3 Precipitate formation evaluation

The fourteen compounds showed pellet formation at 100 µM and 50 µM in the buffer solution by visual inspection (data not shown). Pellets were observed after 40 minutes centrifugation.

3.2.4 Correlation of aggregate formation prediction with experimental data

Among the fourteen compounds, compounds **1**, **2**, **3**, **5**, **6**, **7**, **8**, **9**, **10**, and **13** were predicted to form aggregation or micelle, based on the aggregator advisor tool database. Compound **1** had the highest percentage of similarity to a previously reported aggregator, which was 93% whereas compounds **8** and **13** had the lowest percentage of similarity from the set, which was 72%. Although compounds **11**, **12**, **14** did not resemble any previously described aggregator in the aggregator advisor tool database, it was strongly advised to conduct experimental controls, including aggregation inhibition by the use of a detergent, to confirm whether a compound is acting as an aggregator or not. Compound **4** was the only compound from the list that was not flagged by the aggregator predictor tool (Table 3.6). That being said, the aggregator advisor tool serves as a guidance only, and experiments are the only way to know for sure whether a compound is acting as an aggregator or not. Our results from non-specific inhibition of *Mt*SK by LC-MS, concentration response curves, ^{1}H-NMR spectroscopy, DLS, TEM, precipitate formation evaluation Sections 3.1, 3.1.1, 3.2.1, 3.2.2.1, 3.2.2.2, and 3.2.3, respectively, prove that these compound are aggregators and to correlate them with the prediction data. A percentage of 71.4 was predicted by the aggregator advisor tool to match the experimental data.

Table 3.6. Prediction of aggregate formation compounds by the aggregator advisor tool.

Structure	Aggregate Prediction	*Similarity in percentage
1	Similar to a previously described aggregator.[72]	93%
2	Similar to a previously described aggregator. [72]	77%
3	Similar to a previously described aggregator. [72]	77%
4	It has not been previously described as an aggregator, or it is not similar to an aggregator.	
5	Similar to a previously described aggregator. [72]	73%
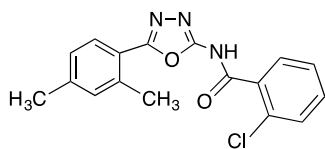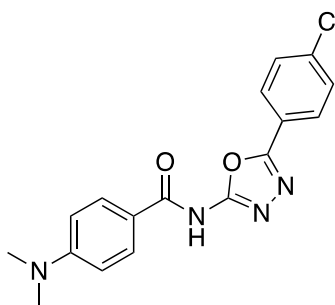
| | Similar to a previously described aggregator.[72] | 81% |
| **6** | | |

| | Similar to a previously described aggregator.[72] | 78% |
| **7** | | |

| | Similar to a previously described aggregator.[72] | 72% |
| **8** | | |

| | Similar to a previously described aggregator.[72] | 87% |
| **9** | | |
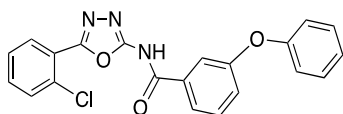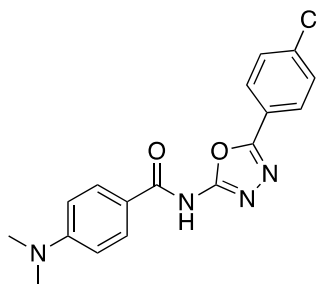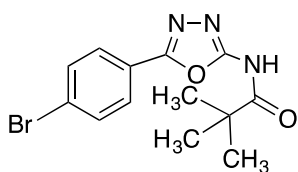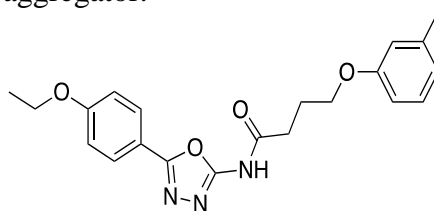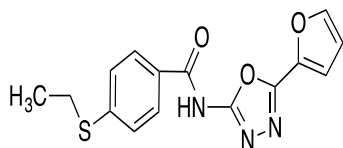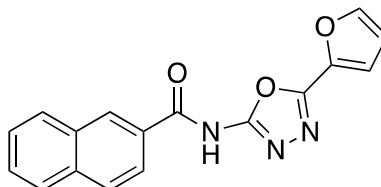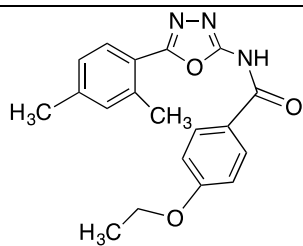
10	Similar to a previously described aggregator.[72]	73%
11	No similarity to any compound that could form aggregates in the aggregator tool predictor database However, but due to high cLogP value of this compound, which is near to many aggregate forming compounds, it is advisable to test it for confirmation.	
12	No similarity to any compound that could form aggregates in the aggregator tool predictor database However, but due to high cLogP value of this compound, which is near to many previously described aggregate forming compounds, it is advisable to test it for confirmation.	
13	Similar to a previously described aggregator.[72]	72%
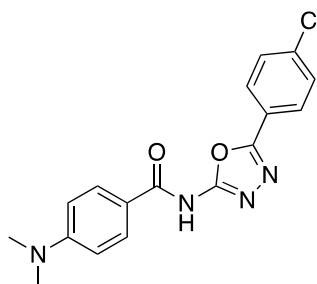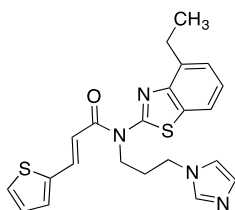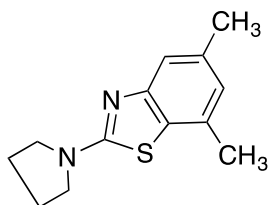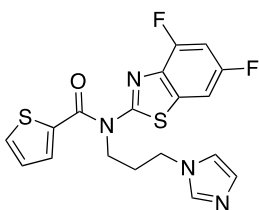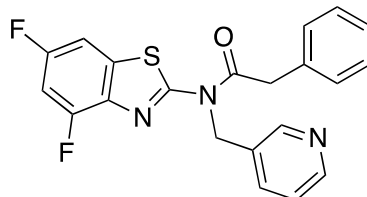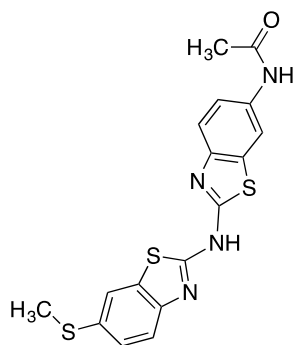
14	No similarity to any compound that could form aggregates in the aggregator tool predictor database However, but due to high cLogP value of this compound, which is near to many previously described aggregate forming compounds, it is advisable to test it for confirmation.

[*] Similarity percentage refers to the similarity in the chemical structure between the compound tested in this study and a previously known aggregator from the literature.

3.3 Correlation of phenotypic activity of oxadiazole-amide and 2-aminobenzothiazole in *Mtb* cell culture with experimental data

All fourteen compounds have been previously tested phenotypically against *M. tuberculosis* H37Rv. The IC_{90} values have been reported to be < 4 µg/ml and the activities of the compounds against *Mtb* were categorized based on their potencies (Table 3.7) [53,62,63]. The results from this study show a lack of correlation with in vivo studies for two reasons. First, since the fourteen compounds have a fairly high cLogP, they are more likely to penetrate the highly lipophilic cell wall of *M. tuberculosis* by passive diffusion and produce their action at any target. This mechanism of transportation for lipophilic drugs was described by Brennan & Nikaido [42]. Second, our findings revealed that these compounds are non-specific binders to *Mt*SK in vitro due to aggregate formation in the aqueous solution, thus discrepancy between in vivo and in vitro results is inevitable.

Table 3.7. Anti-*Mtb* phenotypic activity of oxadiazole-amide and 2-aminobenzothiazole compounds in cell culture

Compound number	TB IC$_{90}$(µg/ml)H37Rv	*Activity level
1	3.04	Medium
2	1.93	Medium
3	1.68	Medium
4	0.69	High
5	3.09	Medium
6	< 0.20	High
7	0.86	High
8	< 0.20	High
9	0.71	High
10	1.8	Medium
11	0.83	High
12	1.75	Medium
13	2.38	Medium
14	< 0.20	High

*Activity level, high: <0.1 – 1.6, medium: 0.9 – 10.3, and low: 6.3 - >50

3.3.1 Correlation of the *Mtb* phenotypic activity with the *Mtb* cell wall permeability prediction

Four descriptors have been used to predict the permeability of the fourteen compounds, including FOSA, cLogP, PISA, and accptHB. Where FOSA refers to the hydrophobic part of the solvent accessible surface area (saturated carbon and attached hydrogen atoms), cLogP is the calculated logarithm of compound's partition coefficient between n-octanol and water, PISA is the portion of the solvent accessible surface area responsible for π interaction, and accptHB is the number of hydrogen bond acceptors. Prediction probabilities were highlighted with three different colors based on their cutoff ranges, including green, orange, and red (Table 3.8). Compounds that displayed a prediction probability of >0.82-1 were considered highly permeable through *Mtb* cell wall and highlighted in green color. Compounds that scored between > 0.55 and <0.82 were considered relatively permeable and highlighted in orange while compounds that showed < 0.55 were considered poorly permeable and marked red. Compounds **11**, **7**, **3**, **6**, **2**, **13**, **9**, and **14** were

predicted to be highly permeable because they displayed prediction values of more than 0.82, whereas compound **10** showed a moderate penetration value of 0.715. Compounds **5**, **8**, **12**, **4**, and **1** expressed low permeability prediction values of less than 0.55. Although the fourteen compounds were active in vivo against *Mtb*, a weak correlation was observed from the results that were obtained by MycPermCheck tool. Compounds **5**, **8**, **12**, **4**, and **1** were considered outliers from the permeability perspective, they displayed high activity profiles phenotypically, which were reflected on their IC$_{90}$ but poor penetration probabilities according to the prediction tool. Furthermore, the compounds that showed high permeability values shared common characteristics, including higher PISA than FOSA, cLogP around 3 and above, and accptHB below 6.5. Therefore, taking into account one descriptor only will not guarantee high permeability values. Instead, all descriptors should be taken into consideration. As described by Merget et al. [66], the computational tool predicts passive diffusion transportation only, which is a limitation of the tool, this suggests that compounds **5**, **8**, **12**, **4**, and **1** transverse *Mtb* cell wall by other mechanisms.

Although the permeability prediction tool is useful for predicting compounds that are expressing their activity through cell wall penetration, absolute confirmation is not expected. Therefore, we suggest that, from the set of 14 compounds, the most active compounds, **4**, **6**, **7**, **8**, **9**, **11**, and **14**, should be further investigated so as to understand their mechanism of action.

Table 3.8. *Mtb* cell wall permeability prediction of oxadiazole-amide and 2-aminobenzothiazole compounds.

Compound number	Prop.	FOSA	LogP	PISA	accptHB	TB IC$_{90}$(μg/m) H37Rv	Activity Level
11	1	201.8	5.148	415.6	6.5	0.83	High
7	1	0	4.446	513.5	5.5	0.86	High
3	0.997	209.1	4.063	355.8	5	1.68	Medium
6	0.966	160.8	3.553	290.3	5	<0.20	High
2	0.991	253.3	4.306	329.3	5.5	1.93	Medium
13	0.998	64.346	4.262	352.16	6.5	2.38	Medium
9	0.87	131.735	2.703	313.41	6	0.71	High

14	0.865	181.64	3.665	263.546	6.5	<0.20	High
10	0.715	301.725	3.728	267.841	5.75	1.8	Medium
5	0.152	160.887	2.206	211.006	6	3.09	Medium
12	0.118	363.259	3.822	92.369	2	1.75	Medium
4	0.057	160.899	1.736	221.912	6.5	0.69	High
1	0.024	391.269	3.637	122.528	5	3.04	Medium
8	0.136	205.122	2.839	173.361	5	< 0.20	High

3.4 Conclusion

In this study, the 14 compounds, oxadiazole-amides and 2-aminobenzothiazole previously shown to be active against *M. tuberculosis* in cell culture and in vitro against *Mt*SK have been characterized as non-specific inhibitors of *Mt*SK. Our findings by the use of LC-MS, ^{1}H-NMR, DLS, TEM, and centrifugation assays suggested that these compounds are non-specific inhibitors of *Mt*SK by aggregate formation. Results from the aggregate formation prediction tool showed that the fourteen compounds except compound **4** may form aggregations in aqueous solution. These predictions, together with the experimental data, confirm that the fourteen synthetic compounds containing oxadiazole-amide and 2-aminobenzothiazole scaffolds are artifactual inhibitors of *Mt*SK. While our findings suggest that these compounds are non-specific inhibitors against *Mt*SK, these compounds displayed activity in *Mtb* cell culture. The correlation of the extent of reported anti-*Mtb* and *Mtb* cell wall permeability prediction tool for the 14 compounds suggest that these compounds are expressing their activities intracellularly due to passive diffusion through cell wall, however, other mechanisms of transportations cannot be excluded.

In general, the assays that were used in this work should serve as practical tools for medicinal chemists to eliminate false positive hits in early drug discovery process. Thus, they will save time, resources, and avoid promiscuous inhibitors. We propose the use of LC-MS and NMR based assays to detect aggregation produced by false positive compounds since both detectors are specific, sensitive, and simple to operate. Also, they are widely used in inhibition studies and routinely available in drug discovery and development laboratories.

REFERENCES

1. World Health Organization (2015) Global tuberculosis control: WHO report Geneva. World Health Organization, Geneva.

2. Centers for Disease Control and Prevention, *Core* Curriculum On Tuberculosis: What The Clinician Should Know. 6th ed. 2013.

3. Shi, L., Eugenin, E. A., & Subbian, S. (2016). Immunometabolism in Tuberculosis. *Frontiers in Immunology*, *7*, 150.

4. Ehlers, S., & Schaible, U. E. (2012). The granuloma in tuberculosis: dynamics of a host pathogen collusion. *Frontiers in Immunology*, *3*, 411.

5. Parrish, N. M., Dick, J. D., & Bishai, W. R. (1998). Mechanisms of latency in *Mycobacterium tuberculosis*. *Trends in Microbiology*, *6*(3), 107–112.

6. Manabe, Y. C., & Bishai, W. R. (2000). Latent *Mycobacterium tuberculosis*-persistence, patience, and winning by waiting. *Nature Medicine*, *6*(12), 1327–1329.

7. Ai, J.-W., Ruan, Q.-L., Liu, Q.-H., & Zhang, W.-H. (2016). Updates on the risk factors for latent tuberculosis reactivation and their managements. *Emerging Microbes & Infections*, *5*, e10.

8. Flynn, J., Chan, J., & Lin, P. (2011). Macrophages and control of granulomatous inflammation in tuberculosis. *Mucosal Immunology*, *4*(3), 271–278.

9. Anishetty, S., Pulimi, M., & Pennathur, G. (2005). Potential drug targets in *Mycobacterium tuberculosis* through metabolic pathway analysis. *Computational Biology and Chemistry*, *29*(5), 368–378.

10. Galperin, M. Y., & Koonin, E. V. (1999). Searching for drug targets in microbial genomes. *Current Opinion in Biotechnology*, *10*(6), 571–578.

11. Sridhar, S., Dash, P., & Guruprasad, K. (2016). Comparative analyses of the proteins from

Mycobacterium tuberculosis and human genomes: Identification of potential tuberculosis

drug targets. *Gene*, *579*(1), 69–74.

12. Parish, T., & Stoker, N. G. (2002). The common aromatic amino acid biosynthesis pathway

    is essential in *Mycobacterium tuberculosis*. *Microbiology. 2002, 148*, 3069–3077.

13. Dhaliwal, B., Nichols, C. E., Ren, J., Lockyer, M., Charles, I., Hawkins, A. R., & Stammers,

    D. K. (2004). Crystallographic studies of shikimate binding and induced conformational

    changes in *Mycobacterium tuberculosis* shikimate kinase. *FEBS Letters*, *574*(1–3), 49–54.

14. Blanco, B., Prado, V., Lence, E., Otero, J. M., Garcia-Doval, C., van Raaij, M. J., Llamas-Saiz,

    A. L., Lamb, H., Hawkins, A. R., González-Bello, C. (2013). *Mycobacterium tuberculosis*

    shikimate kinase inhibitors: design and simulation studies of the catalytic turnover. *Journal of*

    the American Chemical Society, *135*(33), 12366–12376.

15. Maeda, H., & Dudareva, N. (2012). The shikimate pathway and aromatic amino Acid

    biosynthesis in plants. *Annual Review of Plant Biology*, *63*, 73–105.

16. Hartmann, M. D., Bourenkov, G. P., Oberschall, A., Strizhov, N., & Bartunik, H. D. (2006).

    Mechanism of phosphoryl transfer catalyzed by shikimate kinase from Mycobacterium

    tuberculosis. *Journal of Molecular Biology*, *364*(3), 411–423.

17. Krell, T., Coggins, J. R., & Lapthorn, A. J. (1998). The three-dimensional structure of

    shikimate kinase. *Journal of Molecular Biology*, *278*(5), 983–997.

18. R. A. Copeland (2005). Evaluation of enzyme inhibitors in drug discovery. A guide for

    medicinal chemists and pharmacologists. *Methods of Biochemical Analysis, 46*, 1–265.

19. Wunberg, T., Hendrix, M., Hillisch, A., Lobell, M., Meier, H., Schmeck, C., Wild, H.,

    Hinzen, B. Improving the hit-to-lead process: data-driven assessment of drug-like and lead

    like screening hits. *Drug Discovery Today*, 2006, 11, 175–180.

20. Peyressatre, M., Prével, C., Pellerano, M., & Morris, M. C. (2015). Targeting cyclin

dependent kinases in human cancers: From small molecules to peptide inhibitors. *cancers*, *7*(1), 179–237.

21. Zhang, J., Yang, P. L., & Gray, N. S. (2009). Targeting cancer with small molecule kinase inhibitors. *Nature Reviews Cancer*, *9*(1), 28–39.

22. Bajorath, J. (2014). Activity artifacts in drug discovery and different facets of compound promiscuity. *F1000Research*, 3:233.

23. Baell, J. B.; Holloway, G. A. New substructure filters for removal of pan assay interference compounds (PAINS) from screening libraries and for their exclusion in bioassays. J. Med. Chem. 2010, 53, 2719−2740.

24. Davis, B. J., & Erlanson, D. A. (2013). Learning from our mistakes: The "unknown knowns" in fragment screening. *Bioorganic & Medicinal Chemistry Letters*, *23*(10), 2844–2852.

25. Rishton, G. M. Reactive compounds and in vitro false positives in HTS. *Drug Discovery Today*, 1997, 2, 382–384.

26. Shoichet, B. K. (2006). Screening in a spirit haunted world. *Drug Discovery Today*, *11*(13 14), 607–615.

27. Shoichet, B. K. (2006). Interpreting steep dose-response curves in early inhibitor discovery. *Journal of Medicinal Chemistry*, *49*(25), 7274–7277.

28. Baell, J. B., Ferrins, L., Falk, H., & Nikolakopoulos, G. (2013). PAINS: Relevance to tool compound discovery and fragment-based screening. *Australian Journal of Chemistry*, *66*(12), 1483.

29. Pohjala, L., & Tammela, P. (2012). Aggregating behavior of phenolic compounds — A source of false bioassay results? *Molecules*, *17*(9), 10774–10790.

30. Coan, K. E. D., Maltby, D. A., Burlingame, A. L., & Shoichet, B. K. (2009). Promiscuous aggregate-based inhibitors promote enzyme unfolding. *Journal of Medicinal Chemistry*,

52(7), 2067–2075.

31. Seidler, J., McGovern, S. L., Doman, T. N., & Shoichet, B. K. (2003). Identification and prediction of promiscuous aggregating inhibitors among known drugs. *Journal of Medicinal Chemistry*, *46*(21), 4477–4486.

32. Doak, A. K., Wille, H., Prusiner, S. B., & Shoichet, B. K. (2010). Colloid formation by drugs in simulated intestinal fluid. *Journal of Medicinal Chemistry*, *53*(10), 4259–4265

33. Coan, K. E. D., & Shoichet, B. K. (2007). Stability and equilibria of promiscuous aggregates in high protein milieus. *Molecular BioSystems*, *3*(3), 208–213.

34. Coan, K. E. D., & Shoichet, B. K. (2008). Stoichiometry and physical chemistry of promiscuous aggregate-based inhibitors. *Journal of the American Chemical Society*, *130*(29), 9606–9612.

35. Giannetti, A. M., Koch, B. D., & Browner, M. F. (2008). Surface plasmon resonance based assay for the detection and characterization of promiscuous inhibitors. *Journal of Medicinal Chemistry*, *51*(3), 574–580.

36. McGovern, S. L., Caselli, E., Grigorieff, N., & Shoichet, B. K. (2002). A common mechanism underlying promiscuous inhibitors from virtual and high-throughput screening. *Journal of Medicinal Chemistry*, *45*(8), 1712–1722.

37. Chatterjee, D. (1997). The mycobacterial cell wall: structure, biosynthesis and sites of drug action. *Current Opinion in Chemical Biology*, *1*(4), 579–588.

38. Barry, C. E., Lee, R. E., Mdluli, K., Sampson, A. E., Schroeder, B. G., Slayden, R. A., & Yuan, Y. (1998). Mycolic acids: structure, biosynthesis and physiological functions. *Progress in Lipid Research*, *37*(2–3), 143–179.

39. Barry, C. E. (2001). Interpreting cell wall "virulence factors" of *Mycobacterium tuberculosis*. *Trends in Microbiology*, *9*(5), 237–241.

40. Liu, J., Barry, C. E., Besra, G. S., & Nikaido, H. (1996). Mycolic acid structure determines the fluidity of the mycobacterial cell wall. *The Journal of Biological Chemistry*, *271*(47), 29545–29551.

41. Niederweis, M. (2003). Mycobacterial porins--new channel proteins in unique outer membranes. *Molecular Microbiology*, *49*(5), 1167–1177.

42. Brennan, P.J., Nikaido, H. The envelope of mycobacteria. *ANNUAL REVIEW OF BIOCHEMISTRY*. 1995, *64*, 29–63.

43. Sarathy, J. P., Dartois, V., & Lee, E. J. D. (2012). The role of transport mechanisms in *mycobacterium tuberculosis* drug resistance and tolerance. *Pharmaceuticals*, *5*(11), 1210 1235.

44. Gomtsyan, A. (2012). Heterocycles in drugs and drug discovery. *Chemistry of Heterocyclic Compounds*, *48*(1), 7–10.

45. Joshi, S. D., Vagdevi, H. M., Vaidya, V. P., & Gadaginamath, G. S. (2008). Synthesis of new 4-pyrrol-1-yl benzoic acid hydrazide analogs and some derived oxadiazole, triazole and pyrrole ring systems: a novel class of potential antibacterial and antitubercular agents. *European Journal of Medicinal Chemistry*, *43*(9), 1989–1996.

46. Ningaiah, S., Bhadraiah, U. K., Doddaramappa, S. D., Keshavamurthy, S., & Javarasetty, C. (2014). Novel pyrazole integrated 1,3,4-oxadiazoles: Synthesis, characterization and antimicrobial evaluation. *Bioorganic & Medicinal Chemistry Letters*, *24*(1), 245–248.

47. Mamolo, M. G., Zampieri, D., Vio, L., Fermeglia, M., Ferrone, M., Pricl, S., Scilalino, G., Banfi, E. (2005). Antimycobacterial activity of new 3-substituted 5-(pyridin-4-yl)-3H-1,3,4 oxadiazol 2-one and 2-thione derivatives. Preliminary molecular modeling investigations. *Bioorganic & Medicinal Chemistry*, *13*(11), 3797–3809.

48. Andreani, A., Granaiola, M., Leoni, A., Locatelli, A., Morigi, R., & Rambaldi, M. (2001).

Synthesis and antitubercular activity of imidazo[2,1-b]thiazoles. *European Journal of Medicinal Chemistry*, *36*(9), 743–746.

49. Simithy, J., Reeve, N., Hobrath, J. V., Reynolds, R. C., & Calderón, A. I. (2014). Identification of shikimate kinase inhibitors among anti-*Mycobacterium tuberculosis* compounds by LC-MS. *Tuberculosis*, *94*(2), 152–158.

50. Patil, V. S., Nandre, K. P., Ghosh, S., Rao, V. J., Chopade, B. A., Sridhar, B., Bhosale, S. V., Bhosale, S. V. (2013). Synthesis, crystal structure and antidiabetic activity of substituted (E)-3-(Benzo[d]thiazol-2-ylamino) phenylprop-2-en-1-one. *European Journal of Medicinal Chemistry*, *59*, 304–309.

51. Palmer, P. J., Trigg, R. B., & Warrington, J. V. (1971). Benzothiazolines as antituberculous agents. *Journal of Medicinal Chemistry*, *14*(3), 248–251.

52. Abdellatif, K. R. A., Abd El Wareth, G. A., El-Badry, O. M., Ragab, H. M., & El-Enany, M. M. (2015). Synthesis and antimicrobial evaluation of certain purine, benzothiazole and thiazole systems substituted with dialkylaminoalkyl-o-cresols. *Beni-Suef University Journal of Basic and Applied Sciences*, *4*(1), 52–59.

53. Reynolds, R. C., Ananthan, S., Faaleolea, E., Hobrath, J. V., Kwong, C. D., Maddox, C., Rasmussen, L., Sosa, M. I., Thammasuvimol, E., Zhang, W., Secrist, J. A. (2012). High throughput screening of a library based on kinase inhibitor scaffolds against Mycobacterium tuberculosis H37Rv. *Tuberculosis*, *92*(1), 72–83.

54. Yoshida, M., Hayakawa, I., Hayashi, N., Agatsuma, T., Oda, Y., Tanzawa, F., Iwasaki, S., Koyama, K., Furukawa, H., Kurakata, S., Sugano, Y. (2005). Synthesis and biological evaluation of benzothiazole derivatives as potent antitumor agents. *Bioorganic & Medicinal Chemistry Letters*, *15*(14), 3328–3332.

55. Zaoutis, T.E. (2009). Antibiotic resistance: who will pay the bills?. *Clinical Infectious*

Diseases, 49, 11851186.

56. Thammaporn, R., Ishii, K., Yagi-Utsumi, M., Uchiyama, S., Hannongbua, S., & Kato, K. (2016). Mass spectrometric characterization of HIV-1 reverse transcriptase interactions with non-nucleoside reverse transcriptase inhibitors. *Biological & Pharmaceutical Bulletin*, *39*(3), 450–454.

57. Witkowska, H.E., Green, B.N., Carlquist, M. & Shackleton, C.H. (1996) Intact noncovalent dimer of estrogen receptor ligand binding domain can be detected by electrospray ionization mass spectrometry. *Steroids* 61, 433–438.

58. McCullough, B. J., & Gaskell, S. J. (2009). Using electrospray ionisation mass spectrometry to study non-covalent interactions. *Combinatorial Chemistry & High Throughput Screening*, *12*(2), 203–211.

59. Jecklin, M. C., Touboul, D., Bovet, C., Wortmann, A., & Zenobi, R. (2008). Which electrospray-based ionization method best reflects protein-ligand interactions found solution? A comparison of ESI, nanoESI, and ESSI for the determination of dissociation constants with mass spectrometry. *Journal of the American Society for Mass Spectrometry*, *19*(3), 332–343.

60. Woon, E. C. Y., Demetriades, M., Bagg, E. A. L., Aik, W., Krylova, S. M., Ma, J. H. Y., Chang, M., Walport, L. J., Wegman, D. W., Dack, K. N., McDonough, M. A., Krylov, S. N., Schofield, C. J. (2012). Dynamic combinatorial mass spectrometry leads to inhibitors of a 2-oxoglutarate-dependent nucleic acid demethylase. *Journal of Medicinal Chemistry*, *55*(5), 2173–2184.

61. Simithy, J., Gill, G., Wang, Y., Goodwin, D. C., & Calderón, A. I. (2015). Development of an ESI-LC-MS-based assay for kinetic evaluation of *Mycobacterium tuberculosis* shikimate kinase activity and inhibition. *Analytical Chemistry*, *87*(4), 2129–2136.

62. Ananthan, S., Faaleolea, E. R., Goldman, R. C., Hobrath, J. V., Kwong, C. D., Laughon, B. E., Maddry, J. A., Metha, A., Rasmussen, L., Reynolds, R. C., Secrist, J. A., Shindo, N., Show, D. N., Sosa, M. I., White, E. L. (2009). High-throughput screening for inhibitors of Mycobacterium tuberculosis H37Rv. *Tuberculosis*, *89*(5), 334–353.

63. Maddry, J. A., Ananthan, S., Goldman, R. C., Hobrath, J. V., Kwong, C. D., Maddox, C., Rasmussen, L., Reynolds, R. C., Secrist, J. A., Sosa, M. I., White, E.L., Zhang, W. (2009). Antituberculosis activity of the molecular libraries screening center network library. *Tuberculosis*, *89*(5), 354–363.

64. Irwin, J. J., Duan, D., Torosyan, H., Doak, A. K., Ziebart, K. T., Sterling, T., Tumanian, G., Shoichet, B. K. (2015). An aggregation advisor for ligand discovery. *Journal of Medicinal Chemistry*, *58*(17), 7076–7087.

65. Sittiwong, W., Zinniel, D. K., Fenton, R. J., Marshall, D. D., Story, C. B., Kim, B., Lee, J. A., Powers, R., Barletta, R. G., Dussault, P. H. (2014). Development of cyclobutene- and cyclobutane-functionalized fatty acids with inhibitory activity against Mycobacterium tuberculosis. *ChemMedChem*, *9*(8), 1838–1849.

66. Merget, B., Zilian, D., Müller, T., & Sotriffer, C. A. (2013). MycPermCheck: the *Mycobacterium tuberculosis* permeability prediction tool for small molecules. *Bioinformatics* ,*29*(1), 62–68.

67. McGovern, S. L., Helfand, B. T., Feng, B., & Shoichet, B. K. (2003). A Specific Mechanism of Nonspecific Inhibition. *Journal of Medicinal Chemistry*, *46*(20), 4265–4272.

68. Mulabagal, V., & Calderón, A. I. (2010). Development of an ultrafiltration-liquid chromatography/mass spectrometry (UF-LC/MS) Based ligand-binding assay and an LC/MS based functional assay for *Mycobacterium tuberculosis* shikimate kinase. *Analytical Chemistry*, *82*(9), 3616–3621.

69. McGovern, S. L., & Shoichet, B. K. (2003). Kinase inhibitors: not just for kinases anymore. *Journal of Medicinal Chemistry*, *46*(8), 1478–1483.

70. Tomlinson, S. M., & Watowich, S. J. (2012). Use of parallel validation high-throughput screens to reduce false positives and identify novel dengue NS2B-NS3 protease inhibitors. *Antiviral Research*, *93*(2), 245–252.

71. LaPlante, S. R., Carson, R., Gillard, J., Aubry, N., Coulombe, R., Bordeleau, S., Bonneau, P., Little, M., O'Meara, J., Beaulieu, P. L. (2013). Compound aggregation in drug discovery: implementing a practical NMR assay for medicinal chemists. *Journal of Medicinal Chemistry*, *56*(12), 5142–5150.

72. Ferreira, R. S., Simeonov, A., Jadhav, A., Eidam, O., Mott, B. T., Keiser, M. J., McKerrowl, J. H., Maloney, D. J., Irwin, J. J., Shoichet, B. K. (2010). Complementarity between a docking and a high-throughput screen in discovering new cruzain inhibitors. *Journal of Medicinal Chemistry*, *53*(13), 4891–4905.